Development of a new, more regular, mortar method for the coupling of NURBS subdomains within a NURBS patch: Application to a non-intrusive local enrichment of NURBS patches

Robin Bouclier, Jean-Charles Passieux, Michel Salaün

Development of a new, more regular, mortar method for the coupling of NURBS subdomains within a NURBS patch: Application to the non-intrusive local enrichment of NURBS patches

Robin Bouclier[a], Jean-Charles Passieux[b], Michel Salaün[b]

[a] *Université de Toulouse, INSA-Toulouse, IMT UMR CNRS 5219, 135 avenue de Rangueil, F-31077 Toulouse Cedex 04, France*
[b] *Université de Toulouse, INSA/UPS/ISAE/Mines Albi, ICA UMR CNRS 5312 3 rue Caroline Aigle, 31400 Toulouse, France*

Abstract

In this work, we develop a mortar method for the coupling of NURBS subdomains within a NURBS patch that keeps the benefit of using more regular functions. The idea is to use two Lagrange multipliers to match, across the coupling interface, the tractions coming from the discrete displacements in addition to the discrete displacements. It results in a strategy that is suitable with the continuity of the physical solution: when the physical solution is sufficiently smooth, the strategy enables to represent a C^1 behavior; but, when only a C^0 displacement is expected, no additional errors are introduced since only the traction force is continuous and not the whole derivative fields. Lower stress jumps at the coupling interface can then be observed which allows for a better transition of the information. As an application, a non-

Email addresses: bouclier@insa-toulouse.fr (Robin Bouclier), passieux@insa-toulouse.fr (Jean-Charles Passieux), michel.salaun@isae.fr (Michel Salaün)

intrusive algorithm is also built for the proposed coupling method, which enables simple and flexible local enrichments of NURBS patches without loosing the interest of using more regular functions. A range of numerical examples in two-dimensional linear elasticity are carried out along with comparisons with other published NURBS coupling techniques to demonstrate the performance of the proposed coupling and its interest when combined to a non-intrusive strategy.

Keywords: Isogeometric analysis, NURBS, Domain decomposition, Mortar method, Non-intrusive coupling, Non-conforming geometries

1. Introduction

The IsoGeometric Analysis (IGA), which was first introduced in Hughes *et al.* [1] and later developed in Cottrell *et al.* [2], relies on the use of the same functions for the finite element analysis as those used to build the geometry of Computer-Aided Design (CAD) models. Thus, Lagrange polynomials are replaced by Non-Uniform-Rational-B-Splines (NURBS) functions, which constitute the most commonly used technology in CAD. This enables one to deal with both design and analysis using exactly the same geometric models. In addition to the geometric aspect, NURBS functions have a higher order of continuity, namely $C^{(p-1)}$ through the knot-span elements of the mesh for a polynomial degree p, which on a per-degree-of-freedom basis exhibits increased accuracy in comparison to standard Finite Element Methods (FEM) (see, *e.g.*, [3] for a theoretical analysis, [4] for structural vibrations, [5] for standard elasticity, [6] for embedded domain methods and [7, 8] for shell analysis). If the global accuracy of NURBS is now proved, difficulties are still

encountered to integrate different discrete models in a NURBS patch. The reason for this is the rigid tensor product structure of NURBS which necessarily implies a structured quadrangular mesh. As a consequence, the local mesh refinement is not possible directly with the NURBS technology. More generally, the delimitation of a subregion of any shape within a NURBS patch is far from trivial, which prevents from the simple modeling of any specific local behaviors (*e.g.*, introduction of an inclusion [9], crack propagation [11, 10], emergence of a plastic zone [12], ...). Indeed, the basic strategy may involve a re-parametrization of the whole NURBS model, including the splitting of the new geometry into several patches with C^0 continuity at the boundaries. This entails a considerable modeling effort which is often as complex and time consuming as standard mesh generation and then, is opposed to the core idea of IGA.

To answer the issue of local mesh refinement, numerous research works have been dedicated to the construction of new splines these last years. To start with, one may cite the hierarchical B-splines and NURBS [13, 14, 15]. These new splines are easy to implement but the local mesh refinement still seems to spread for higher-order functions. With similar properties, one may also cite the development of LRB-splines [16] and multigrids-based NURBS [20]. Alternatively, another technology seems to have gathered an important momentum from both the computational geometry and analysis communities : the so-called T-splines [17, 18, 19]. In addition to be efficient for local mesh refinement, the T-splines also appear suitable to address trimmed multi-patch geometries. However, the implementation can appear complex and additional efforts may be necessary for the more general

situations mentioned above (modeling of an inclusion, local fracture, local plasticity).

To circumvent the problem, the purpose of this work is to develop a coupling method that is able to connect different NURBS subdomains within a global NURBS patch. Regarding NURBS coupling, many attempts have been devoted these last five years to the connection of NURBS patches to foster the study of multi-patch geometries. Certainly one of the first works on the subject was that of Hesch and Betsch [21], who used a Lagrange multiplier field to add the work performed by coupling tractions along the interface to the weak form. In the framework of NURBS Lagrange multiplier methods, one may also cite the work of Brivadis *et al.* [22] where several choices of Lagrange multiplier spaces are investigated theoretically and numerically. Then, a comparative numerical study in Apostolatos *et al.* [23] showed the efficiency of a Nitsche-based technique for NURBS. Nitsche coupling has subsequently been used for connecting 3D NURBS patches [9], for 3D-plate NURBS coupling [24, 25], and with NURBS immersed boundary methods [26]. Even if it may appear interesting due to the absence of additional degrees of freedom, the Nitsche method leads to a comparatively high computational effort since an additional eigenvalue problem has to be solved for the stabilizing term. As a result, Dornisch *et al.* [27] developed a weak substitution method to simplify the implementation and reduce the computational cost. From this overview, it may be noticed that most of the coupling techniques elaborated for NURBS nowadays are dedicated to the connection of NURBS patches, *i.e.*, the coupling along a C^0 interface. Unlike these works, we are interested here in a method suitable for the coupling of

NURBS subdomains within a NURBS patch, *i.e.*, where the continuity of the basis functions is expected to be higher than C^0. As a result, the objective of our work is to develop a coupling formulation that makes use of the higher-order continuity achieved by the NURBS functions. In particular, the better representation of the derivative fields offered by NURBS is of importance.

When applied to perform local enrichment, an interesting feature of a coupling method may be its ability to be implemented using a non-intrusive strategy. Roughly speaking, a method is said to be non-intrusive when its implementation is very simple from existing techniques and numerical codes. In the context of standard FEM, a group of global/local coupling methods, classified as non-intrusive, has emerged these last years. Based on the idea of Whitcomb [28] and formalized later in Gendre *et al.* [12] for the modeling of local plasticity, these methods involve the definition of two finite element models: a global coarse model of the whole structure and a local more detailed "submodel" meant to replace the global model in the area of interest. An iterative coupling technique is used to perform the substitution in an exact but non-intrusive way: only interface data are transmitted from one model to the other and the global stiffness operator remains unchanged (independently from the shape of the local domain). The performance of such a strategy has been highlighted in many applications (see, *e.g.*, [11] for the modeling of crack propagation, [29] for the modeling of localized uncertainties, [30] for 3D-plate coupling and [31] for nonlinear domain decomposition). More recently, an extension in the NURBS context has been proposed in Bouclier *et al.* [32] and has proved to be a good candidate for NURBS local enrichment. Among the advantages, one may cite the elimination of costly

NURBS re-parametrization procedures for the global model (even if the local area evolves), the possibility to assemble and factorize the global stiffness operator only once, the good conditioning of the systems to be solved, and the easy merging for a NURBS code with any other specific numerical codes. However, the coupling method used in this contribution was the classical one and thus, only a C^0 continuity across the coupling interface was ensured. As a result, the goal of the present work is not only to develop a coupling method suitable with the higher-order continuity of NURBS, but also to be able to implement it in a non-intrusive way to perform NURBS local enrichment.

In this context, we propose in this paper a coupling method in which the tractions coming from the discrete displacements are matched, in addition to the usual discrete displacements, across the coupling interface. It results in a strategy able to represent a C^1 behavior at the interface but also suitable to capture a C^0 displacement (such as in the case of bi-material structures for example). The reason for this is that only physical quantities are transmitted from one model to the other. To meet the non-intrusive aspect, a Lagrange multiplier approach is followed. More precisely, two Lagrange multipliers are introduced to ensure the two coupling constraints. We believe that the proposed method is more consistent with the analysis properties of IGA since it allows for a smoother representation of the solution across the coupling interface.

The paper is organized as follows: first a brief review of IGA with NURBS is given and the reference coupling problem to be solved is presented in Section 2; after reviewing the classical NURBS approaches, the new coupling method is constructed in Section 3; then, the associated iterative non-

intrusive algorithm is built in Section 4; Section 5 presents a set of numerical experiments in two-dimensional linear elasticity to assess the performance of our methodology; finally, concluding remarks are formulated in section 6.

2. The reference NURBS domain decomposition problem

This section establishes the context of the study and introduces the corresponding notations. First, a brief review of the concept of NURBS-based IGA is provided and the difficulty to integrate different discrete models in different regions of a NURBS patch is highlighted. Then, the reference domain decomposition problem along with its governing equations and its weak form is presented.

2.1. Isogeometric analysis based on NURBS

For the discretization of the problem, the recent concept of IGA based on NURBS functions is used. Let us start by briefly reviewing the concept. Only the fundamentals are given here. For further details, the interested reader is referred to the references cited below.

The NURBS concept was first introduced in Hughes *et al.* [1] and formalized more recently in the book by Cottrell *et al.* [2]. NURBS functions are a generalized version of B-spline functions and have become a standard for geometric modeling in CAD and computer graphics (see, for example, Cohen *et al.* [33], Piegl and Tiller [34], Farin [35] and Rogers [36]). These functions lend themselves to an exact representation of many shapes used in engineering, such as conical sections. They can be viewed as rational projections of higher-order B-splines and, therefore, they possess many of the properties of B-splines, the most interesting one being their high degree of continuity.

For the presentation in this section, we consider a domain in 3D so as to be general. If $N_A, A \in \{1, 2, .., n\}$ denote the n 3D NURBS functions, $\omega_A, A \in \{1, 2, .., n\}$ the associated weights and $P_A, A \in \{1, 2, .., n\}$ the associated control points of coordinates $\mathbf{x}_A$ in the global coordinate system, the geometry of the structure is described through the position vector $\mathbf{M}$ defined as:

$$\mathbf{M} = \sum_{A=1}^{n} N_A \mathbf{x}_A, \tag{1}$$

where the NURBS functions are obtained from the B-spline functions $\overline{N}_A, A \in \{1, 2, .., n\}$ such that:

$$N_A = \frac{\overline{N}_A w_A}{\sum_{A=1}^{n} \overline{N}_A w_A}. \tag{2}$$

Now, all one needs to do in order to define the 3D B-spline functions $\overline{N}_A$ at control point P_A is to perform the tensor product of the 1D B-spline functions associated with this point in the three spatial directions. If one denotes $M_i^1, i \in \{1, 2, .., n_1\}$, $M_j^2, j \in \{1, 2, .., n_2\}$ and $M_k^3, k \in \{1, 2, .., n_3\}$ the n_1, n_2 and n_3 1D B-spline functions associated with each of the three spatial directions, this means that at control point P_A, which corresponds to the i^{th}, j^{th} and k^{th} control points in these directions, one has:

$$\overline{N}_A = M_i^1 \times M_j^2 \times M_k^3. \tag{3}$$

The 1D B-spline functions are defined using a knot vector. Each knot vector associated with a direction is defined in the parametric domain. For example, for the first direction, one takes knot vector $\Xi = \{\xi_1, \xi_2, .., \xi_{n_1+p+1}\}$, where $\xi_l \in \mathbb{R}$ is the l^{th} knot, with l being the knot index ($l \in \{1, 2, .., n_1 + p + 1\}$)

and p the polynomial degree of the functions $M_i^1, i \in \{1, 2, .., n_1\}$. The knots divide the parametric space into knot-span elements. In the following, the knot-span elements will be also simply denoted by the elements. The interval $[\xi_1, \xi_{n_1+p+1}]$ constitutes the NURBS patch. Thus, unlike standard FEM where each element has its own parametrization, the parametric space of B-Spline functions is localized onto the patch. The patch may be seen as a macro-element. Many geometries utilized for academic test cases can be modelled with a single patch. In two-dimensional topologies, a patch is a rectangle in the parametric domain. In three dimensions it is a cuboid.

There can be more than one knot at a given location of the parametric space. If m is the multiplicity of the considered knot, the functions have C^{p-m} continuity at that location. Thus, for quadratic and higher-order NURBS, the continuity at the elements boundaries at the interior of the NURBS patch is expected to be higher than the classical C^0 regularity encountered in standard FEM. If the knots are evenly spaced, the knot vector is said to be uniform. A knot vector whose first and last knots have multiplicity $p + 1$ is said to be open. In this case, the basis is interpolating at the boundary nodes of the interval, which facilitates the application of the boundary conditions. Only open uniform knot vectors will be considered in this work. The 1D B-spline basis functions for a given order p are defined recursively from the knot vector using the Cox-de Boor recursion formula (see, for example, Cohen *et al.* [33]). To take advantage of the superior approximation properties of NURBS functions, we choose them to be at least of polynomial degree two in the three spatial directions. As far as continuity is concerned, we perform k-refinement, meaning that we add elements while keeping the higher

degree of continuity of the NURBS functions, namely C^{p-1} at the knot level. The positions of the control points and the values of the associated weights can be adjusted in order to build conical sections exactly, after which these geometries are preserved through mesh refinement. For a good overview of mesh generation and refinement, see Cottrell *et al.* [37].

The tensor product nature of NURBS shape functions (see Eq. (3)) makes it difficult to handle localized phenomena within the NURBS patch. In other words, we necessarily end up with a structured quadrangular mesh in a NURBS patch. For example, this makes the local mesh refinement impossible directly (see, *e.g.*, [15] for completeness). More generally, this makes the integration of a subregion (of any shape) within a NURBS patch far from trivial. Indeed, since standard IGA technology requires a boundary fitted discretization for the analysis, a re-parametrization of the whole NURBS model taking into account the subregions may be required. This may lead to the splitting of the new geometry into several patches with C^0 continuity at the boundaries. This entails a considerable modelling effort, which is often as complex and time consuming as standard mesh generation. More details regarding this issue can be found in [26, 32].

2.2. The NURBS domain decomposition problem

To circumvent the problem of the integration of subregions within a NURBS patch, it is proposed in this work to develop a coupling method that is able to connect different NURBS subdomains within a global NURBS patch. The corresponding domain decomposition problem to be solved is introduced in the following.

2.2.1. Governing equations.

We consider in this work the case of multi-domain linear elasticity in $\Omega \subset \mathbb{R}^d$, $d = 2$ or 3 being the dimension of the problem. Domain Ω constitutes the NURBS patch to be decomposed into subdomains. For simplicity in the presentation, we assume that Ω is divided into only two disjoint, open and bounded subsets Ω_{11} and Ω_2 such that $\Omega = \Omega_{11} \cup \Omega_2$ and $\Omega_{11} \cap \Omega_2 = \varnothing$. Those two non-overlapping subdomains share a common interface denoted Γ (see Fig. 1). Domains Ω_{11} and Ω_2 are subjected to body forces $\mathbf{f}_{11}^{\mathbf{g}}$ and $\mathbf{f}_{2}^{\mathbf{g}}$, respectively. Furthermore, forces $\mathbf{F}_{11}^{\mathbf{g}}$ and $\mathbf{F}_{2}^{\mathbf{g}}$ are associated to boundaries $\Gamma_{F_{11}}$ and Γ_{F_2} and, displacements $\mathbf{u}_{11}^{\mathbf{g}}$ and $\mathbf{u}_{2}^{\mathbf{g}}$ are prescribed over boundaries $\Gamma_{u_{11}}$ and Γ_{u_2}. The boundaries satisfy the following relations :

$$\begin{cases} \Gamma_{F_m} \cup \Gamma_{u_m} \cup \Gamma = \partial\Omega_m \\ \Gamma_{F_m} \cap \Gamma_{u_m} = \varnothing \\ \Gamma_{F_m} \cap \Gamma = \varnothing \\ \Gamma_{u_m} \cap \Gamma = \varnothing \end{cases} \quad \text{with} \quad m = 11 \text{ and } 2.$$

Remark 1. *As subdomains are open, one would need to write* $\Omega = \overbrace{\overline{\Omega}_{11} \cup \overline{\Omega}_2}^{\text{o}}$ *to be rigorous with the boundary* Γ*. In the paper, we decide to omit this notation for the sake of readability.*

Remark 2. *Regarding the notation, the reason why we use* Ω_{11} *and* Ω_2 *for the subdomains instead of* Ω_1 *and* Ω_2 *will appear in section 4.*

Regarding the NURBS discretization, domains Ω_{11} and Ω_2 are composed of several NURBS knot-span elements (or pieces of knot-span elements). In

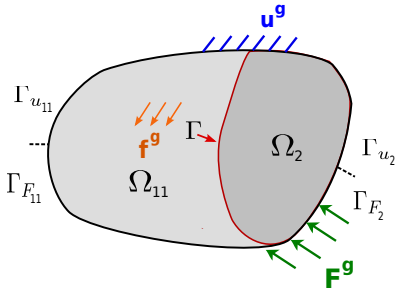

Figure 1: Reference domain decomposition problem.

practice, these regions are built by extracting a central zone from a larger NURBS patch made of open knot vectors (as it is done in hierarchical approaches [13, 14, 15, 20]). The principle of such constructions is illustrated in Fig. 2 for the two-dimensional case. The figure shows the parametric spaces of three different domain decomposition problems. On these examples, we start by defining several discretizations of the global NURBS patch in Ω and then, we extract the regions that compose the subdomains. The associated one-dimensional case with quadratic B-Spline basis functions is added in Fig. 2(a). For each subdomain, the control points that are associated to the basis functions whose support is not in the subdomain are removed. We notice that an identical procedure is used in Chemin *et al.* [20] to construct the local NURBS grids of the multigrid algorithm. Depending on the NURBS discretization of the two subdomains along the interface Γ, three coupling situations are possible:

1. The coupling of matching meshes (see Fig. 2(a)): in this case, the interface Γ is aligned with the edges of the elements in the two subdomains and the meshes of the two subdomains along the interface are perfectly aligned.

2. The coupling of non-matching meshes (see Fig. 2(b)): in this case, the interface Γ is aligned with the edges of the elements in the two subdomains but the meshes of the two subdomains along the interface are not aligned.
3. The coupling of non-conforming geometries (see Fig. 2(c)): in this case, the interface Γ is not aligned with the edges of the elements which means that some knot-span elements are overlapped.

From such constructions, it results that the continuity of the basis functions of the two subdomains at the coupling interface Γ is higher than C^0 (provided quadratic (or higher-order) NURBS basis functions are used). This is in contrast with the more usual situation of the coupling of IGA patches which is achieved along C^0 interfaces (see, *e.g.*, [9, 22, 23, 26, 27]).

Remark 3. *Starting with the whole global NURBS patch and then extracting the discretizations of the subdomains as illustrated in Fig. 2 may not be necessary in practice. Indeed, to ensure a higher-order continuity of the functions at the coupling interface, only a few additional knot-span elements have to be considered at the exterior of the interface coupling. For example, in the case of conforming geometries (see Fig. 2(a) and 2(b)), only p additional knot-span elements are required to reach a C^{p-1} continuity at the interface.*

Remark 4. *Regarding local mesh refinement, it may be noted from the three coupling cases presented above that we undertake to solve more general situations than the ones classically encountered with hierarchical B-Splines and NURBS. Indeed, the usual IGA hierarchical approaches are often restricted to the situation of conforming geometries.*

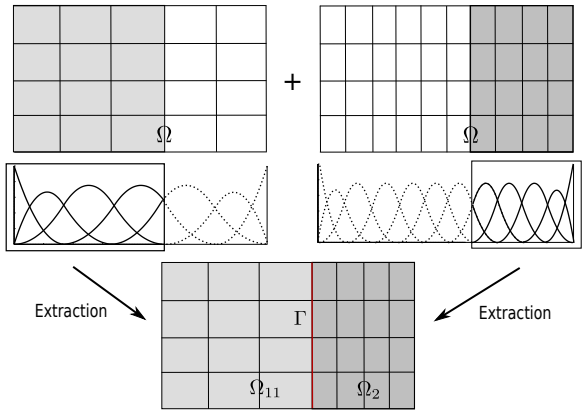

(a) Coupling of matching meshes.

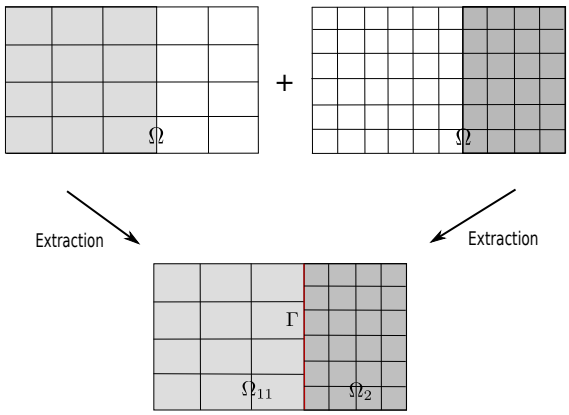

(b) Coupling of non-matching meshes.

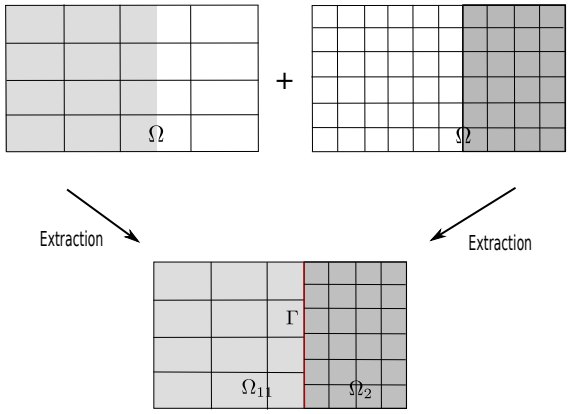

(c) Coupling of non-conforming geometries

Figure 2: NURBS discretizations of the domain decomposition problem: illustrations in the parametric space.

The problem to be solved is a classical two-domain linear elastic problem in $\Omega_{11} \cup \Omega_2$. In each subdomain, the kinematic constraints, the equilibrium equations and the constitutive relations have to be verified. Using the subscript m to denote a quantity that is valid over region Ω_m, with $m = 11$ and 2, the corresponding governing equations read:

$$\begin{cases} \mathbf{u}_{\mathrm{m}} = \mathbf{u}_{\mathrm{m}}^{\mathbf{g}} \quad \text{over} \quad \Gamma_{u_{\mathrm{m}}} \ ; \\ \mathbf{div}(\underline{\underline{\sigma_{\mathrm{m}}}}) + \mathbf{f}_{\mathrm{m}}^{\mathbf{g}} = \mathbf{0} \quad \text{in} \quad \Omega_{\mathrm{m}} \ ; \\ \underline{\underline{\sigma_{\mathrm{m}}}} \ \mathbf{n}_{\mathrm{m}} = \mathbf{F}_{\mathrm{m}}^{\mathbf{g}} \quad \text{over} \quad \Gamma_{F_{\mathrm{m}}} \ ; \\ \underline{\underline{\sigma_{\mathrm{m}}}} = \underline{\underline{\underline{\underline{C_{\mathrm{m}}}}}} \ \underline{\underline{\varepsilon}}(\mathbf{u}_{\mathrm{m}}) \quad \text{in} \quad \Omega_{\mathrm{m}}. \end{cases} \tag{4}$$

For the sake of readability, we decided to use bold symbols for vectors while we underline twice the second- and four times the fourth-order tensors. In the above equations, $\underline{\underline{\varepsilon}}(\mathbf{u}_{\mathrm{m}})$ denotes the infinitesimal strain tensors, $\underline{\underline{\sigma_{\mathrm{m}}}}$ the Cauchy stress tensors and $\underline{\underline{\underline{\underline{C_{\mathrm{m}}}}}}$ the Hooke tensors. $\mathbf{n}_{11}$ and $\mathbf{n}_2$ represent the outward unit normals to Ω_{11} and Ω_2, respectively. For the coupling interface, the continuity of the displacements:

$$\mathbf{u}_{11} - \mathbf{u}_2 = \mathbf{0} \quad \text{on} \quad \Gamma \ ; \tag{5}$$

and the equilibrium of the traction forces:

$$\underline{\underline{\sigma_{11}}}\mathbf{n}_{11} + \underline{\underline{\sigma_2}}\mathbf{n}_2 = \mathbf{0} \quad \text{on} \quad \Gamma \ ; \tag{6}$$

have to be ensured. In the following, we will consider the unit normal vector $\mathbf{n}$ over the interface Γ such that $\mathbf{n} = \mathbf{n}_{11}|_\Gamma = -\mathbf{n}_2|_\Gamma$.

2.2.2. Weak form of the problem.

Let us introduce the subspaces of $[H^1(\Omega)]^d$ needed for the weak equilibrium of the complete domain Ω, namely:

$$\begin{aligned} \mathcal{U} &= \left\{ \mathbf{u} \in \left[H^1(\Omega)\right]^d,\ \mathbf{u}|_{\Gamma_{u11}} = \mathbf{u}_{11}^{\mathbf{g}} \text{ and } \mathbf{u}|_{\Gamma_{u_2}} = \mathbf{u}_2^{\mathbf{g}} \right\} \quad ; \\ \mathcal{V} &= \left\{ \mathbf{v} \in \left[H^1(\Omega)\right]^d,\ \mathbf{v}|_{\Gamma_{v_{11}}} = \mathbf{0} \text{ and } \mathbf{v}|_{\Gamma_{u_2}} = \mathbf{0} \right\}. \end{aligned} \tag{7}$$

Using the principle of virtual work, we obtain the variational form of the elasticity problem (4)-(6), as follows:

$$\begin{cases} \text{Find } \mathbf{u} \in \mathcal{U} \text{ such that:} \\ a(\mathbf{u}, \mathbf{v}) = l(\mathbf{v}), \quad \forall \mathbf{v} \in \mathcal{V}, \end{cases} \tag{8}$$

where the bilinear form a and the linear form l read:

$$\begin{cases} a(\mathbf{u}, \mathbf{v}) = \displaystyle\sum_{m=11,2} a_m(\mathbf{u}_{\mathrm{m}}, \mathbf{v}_{\mathrm{m}}) = \sum_{m=11,2} \int_{\Omega_m} \underline{\underline{\varepsilon}}(\mathbf{v}_{\mathrm{m}}) : \underline{\underline{\underline{\underline{C_m}}}}\, \underline{\underline{\varepsilon}}(\mathbf{u}_{\mathrm{m}})\, \mathrm{d}\Omega_m \ ; \\ l(\mathbf{v}) = \displaystyle\sum_{m=11,2} l_m(\mathbf{v}_{\mathrm{m}}) = \sum_{m=11,2} \int_{\Omega_m} \mathbf{v}_{\mathrm{m}} \cdot \mathbf{f}_{\mathrm{m}}^{\mathbf{g}} \mathrm{d}\Omega_m + \int_{\Gamma_{F_m}} \mathbf{v}_{\mathrm{m}} \cdot \mathbf{F}_{\mathrm{m}}^{\mathbf{g}} \mathrm{d}\Gamma_{F_m}. \end{cases} \tag{9}$$

3. The proposed coupling method

In this part, the proposed coupling method is presented first under its variational continuum form and then under its discrete form. For a better understanding of the new method, we first recall in the variational setting two strategies that have been classically used in IGA: the mortar coupling (see, *e.g.*, [22, 23]) and the Nitsche coupling (see, *e.g.*, [23, 9, 24, 26, 25]). To avoid confusion with the newly developed method, we denote these established strategies by the "classical mortar coupling" and the "classical Nitsche

coupling", respectively.

3.1. The continuum version

We now regard the coupling problem (4)-(6) as a two-domain elasticity problem with mutually influencing boundary conditions along the common coupling interface Γ. We thus start by defining the functional spaces $\mathcal{U}_{\mathrm{m}}$ and $\mathcal{V}_m$ over domain Ω_m that will contain the solution and trial functions respectively:

$$\mathcal{U}_{\mathrm{m}} = \left\{ \mathbf{u}_{\mathrm{m}} \in \left[H^1 \left(\Omega_m \right) \right]^d, \ \mathbf{u}_{\mathrm{m}}|_{\Gamma_{u_m}} = \mathbf{u}_{\mathrm{m}}^{\mathbf{g}} \right\} \ ; \ \mathcal{V}_m = \left\{ \mathbf{v}_{\mathrm{m}} \in \left[H^1 \left(\Omega_m \right) \right]^d, \ \mathbf{v}_{\mathrm{m}}|_{\Gamma_{u_m}} = \mathbf{0} \right\}. \tag{10}$$

We recall that the subscript $m \in \{11, 2\}$ denotes a quantity that is valid over domain Ω_m.

3.1.1. A review of the classical mortar approach.

In the context of mortar approaches or, in other words, in the context of Lagrange multiplier methods, a mixed formulation is set up to impose the coupling constraints (5) and (6). Classically, a single Lagrange multiplier $\boldsymbol{\lambda} \in \mathcal{M}$ (where $\mathcal{M}$ is an appropriate space) is introduced, as the dual unknown, to represent both of the interface traction forces, *i.e.*, $\underline{\underline{\sigma_{11}}}\mathbf{n} = \underline{\underline{\sigma_2}}\mathbf{n} = -\boldsymbol{\lambda}$ in Eq. (6). Then, the interface Dirichlet condition (5) is imposed in a weak sense over Γ using the Lagrange multiplier. This leads to the formulation of the following Lagrangian of the coupled problem:

$$L_{\mathrm{basic}}\Big((\mathbf{u}_{11}, \mathbf{u}_2), \boldsymbol{\lambda} \Big) = \frac{1}{2} a_{11} \left(\mathbf{u}_{11}, \mathbf{u}_{11} \right) + \frac{1}{2} a_2 \left(\mathbf{u}_2, \mathbf{u}_2 \right) - l_{11} \left(\mathbf{u}_{11} \right) - l_2 \left(\mathbf{u}_2 \right) + b \left(\boldsymbol{\lambda}, \mathbf{u}_{11} - \mathbf{u}_2 \right). \tag{11}$$

Bilinear forms a_m and linear forms l_m are given in Eq. (9) and bilinear form b is defined such that:

$$b\left(\boldsymbol{\mu}, \mathbf{u}\right) = \int_{\Gamma} \boldsymbol{\mu} \cdot \mathbf{u} \mathrm{d}\Gamma. \tag{12}$$

With above developments, we can finally obtain the classical mortar coupling formulation of the reference problem as follows:

$$\boxed{\begin{array}{l} \text{Find } \mathbf{u}_{11} \in \mathcal{U}_{11},\ \mathbf{u}_2 \in \mathcal{U}_2, \text{ and } \boldsymbol{\lambda} \in \mathcal{M} \text{ such that:} \\ \left\{ \begin{array}{l} a_{11}\left(\mathbf{u}_{11}, \mathbf{v}_{11}\right) + b(\boldsymbol{\lambda}, \mathbf{v}_{11}) = l_{11}\left(\mathbf{v}_{11}\right), \quad \forall \mathbf{v}_{11} \in \mathcal{V}_{11}\ ; \\ a_2\left(\mathbf{u}_2, \mathbf{v}_2\right) - b(\boldsymbol{\lambda}, \mathbf{v}_2) = l_2\left(\mathbf{v}_2\right), \quad \forall \mathbf{v}_2 \in \mathcal{V}_2\ ; \\ b(\boldsymbol{\mu}, \mathbf{u}_{11} - \mathbf{u}_2) = 0, \quad \forall \boldsymbol{\mu} \in \mathcal{M}. \end{array} \right. \end{array}} \tag{13}$$

One advantage of such a formalism is that within its discrete form, it enables to keep separated and unmodified the stiffness operators associated to the subdomains. Indeed, the communication between the subdomains is performed via the Lagrange multiplier only. This feature is the basis of the non-overlapping domain decomposition methods developed for high performance computing on parallel computer architectures (see, *e.g.*, [38, 39, 40]). In the same idea, such a property enables to build non-intrusive coupling algorithms for the modeling of local behaviors (see, *e.g.*, [12, 11, 30, 31, 32]). Several numerical codes can then be coupled in an iterative way with the exchange of only interface data to carry out the global/local simulation. However, the drawback of such a formulation is that a special care may be required for the construction of the approximation space of $\mathcal{M}$ to avoid undesirable energy-free oscillations (due to the non-satisfaction of the *inf-sup* condition).

3.1.2. A review of the classical Nitsche approach.

Conversely, in the Nitsche coupling technique, the stiffness operators of the different subdomains are merged together which eliminates the need of additional degrees of freedom. A connection between Nitsche and Lagrange multiplier couplings can be made (see, *e.g.*, [41, 42]). Starting with the Lagrange multiplier method, the idea to obtain the Nitsche method is to replace the Lagrange multiplier by the mean interface resultant force coming from the displacement. We therefore define the average of the stresses and of the virtual stresses on the interface as follows:

$$\begin{cases} \left\{\underline{\underline{\sigma}}\right\} = \left(\gamma \underline{\underline{\sigma_{11}}}\left(\mathbf{u}_{11}\right) + (1-\gamma)\underline{\underline{\sigma_2}}\left(\mathbf{u}_2\right)\right)|_\Gamma = \left(\gamma \underline{\underline{\underline{\underline{C_{11}}}}}\,\underline{\underline{\varepsilon}}\left(\mathbf{u}_{11}\right) + (1-\gamma)\underline{\underline{\underline{\underline{C_2}}}}\,\underline{\underline{\varepsilon}}\left(\mathbf{u}_2\right)\right)|_\Gamma \\ \left\{\underline{\underline{\tau}}\right\} = \left(\gamma \underline{\underline{\sigma_{11}}}\left(\mathbf{v}_{11}\right) + (1-\gamma)\underline{\underline{\sigma_2}}\left(\mathbf{v}_2\right)\right)|_\Gamma = \left(\gamma \underline{\underline{\underline{\underline{C_{11}}}}}\,\underline{\underline{\varepsilon}}\left(\mathbf{v}_{11}\right) + (1-\gamma)\underline{\underline{\underline{\underline{C_2}}}}\,\underline{\underline{\varepsilon}}\left(\mathbf{v}_2\right)\right)|_\Gamma \end{cases}$$
$$\text{with} \quad \gamma \in [0,1]\,. \tag{14}$$

We note that in most situations (particularly when the material properties of the subdomains to couple are close), $\gamma = 1/2$ is considered. Denoting now the jump of the displacements and of the virtual displacements on the interface such as:

$$[\![\mathbf{u}]\!] = \left(\mathbf{u}_{11} - \mathbf{u}_2\right)_\Gamma \quad \text{and} \quad [\![\mathbf{v}]\!] = \left(\mathbf{v}_{11} - \mathbf{v}_2\right)_\Gamma\,, \tag{15}$$

we obtain the following Nitsche bilinear form:

$$a_{\mathrm{N}}\Big((\mathbf{u}_{11}, \mathbf{u}_2), (\mathbf{v}_{11}, \mathbf{v}_2) \Big) = a_{11}(\mathbf{u}_{11}, \mathbf{v}_{11}) + a_2(\mathbf{u}_2, \mathbf{v}_2) - \int_\Gamma [\![\mathbf{u}]\!] \cdot \{\underline{\underline{\tau}}\}\, \mathbf{n} \mathrm{d}\Gamma - \int_\Gamma \{\underline{\underline{\sigma}}\}\, \mathbf{n} \cdot [\![\mathbf{v}]\!] \mathrm{d}\Gamma. \tag{16}$$

This bilinear form needs finally to be enriched with a stabilization term to ensure the ellipticity of the boundary value problem. Denoting the stabilization parameter by α, the stabilized variational formulation of the problem using the classical Nitsche approach can be written as follows:

$$\boxed{\begin{array}{l} \text{Find } (\mathbf{u}_{11}, \mathbf{u}_2) \in \mathcal{U}_{11} \times \mathcal{U}_2, \text{ such that:} \\ a_{\mathrm{N}}\Big((\mathbf{u}_{11}, \mathbf{u}_2), (\mathbf{v}_{11}, \mathbf{v}_2) \Big) + \alpha \displaystyle\int_\Gamma [\![\mathbf{u}]\!] \cdot [\![\mathbf{v}]\!] \mathrm{d}\Gamma = l_{11}(\mathbf{v}_{11}) + l_2(\mathbf{v}_2), \quad \forall (\mathbf{v}_{11}, \mathbf{v}_2) \in \mathcal{V}_{11} \times \mathcal{V}_2. \end{array}} \tag{17}$$

While in formulation (13) a suitable approximation space for the Lagrange multiplier needs to be chosen, the Nitsche approach (17) requires the choice of a suitable value for α. It has been shown that an estimation of α can be obtained by solving a generalized eigenvalue problem [23, 9] (or several local eigenvalue problems [26]) over the interface.

3.1.3. The newly-developed mortar approach.

In the two coupling formulations presented above, we notice that the property of higher-order continuity of the NURBS basis functions at the interface Γ has not been used. Indeed, if the continuity of the discrete displacement is enforced across Γ, there is no reason with such formulations that the interface traction force coming from the discrete displacement is continuous through the interface. In other words, there is no reason that the discrete

displacement solution satisfies:

$$\left(\underline{\underline{\sigma_{11}}}(\mathbf{u}_{11})\mathbf{n} - \underline{\underline{\sigma_2}}(\mathbf{u}_2)\mathbf{n}\right)|_\Gamma = \left(\underline{\underline{\underline{\underline{C_{11}}}}}\,\underline{\underline{\varepsilon}}(\mathbf{u}_{11})\mathbf{n} - \underline{\underline{\underline{\underline{C_2}}}}\,\underline{\underline{\varepsilon}}(\mathbf{u}_2)\mathbf{n}\right)|_\Gamma = \mathbf{0}. \tag{18}$$

However, it has to be noted that such an equality is verified by a single NURBS patch solution and that such a constraint seems to have a physical meaning according to Eq. (6) of our reference problem. As result, we propose in this work to add constraint (18) in our solution space $\mathcal{U}$ and virtual space $\mathcal{V}$ (see, eq. (7)). We emphasize that such a treatment seems to be consistent here because the interpolated functions are more regular (at least C^1), which implies that the gradients of the displacement, and so the stresses and tractions forces, are defined at the coupling interface.

To take into account the additional constraint in our coupling formulation, we propose to follow a Lagrange multiplier strategy since the intended application of this work is the non-intrusive local enrichment of NURBS patches. Two Lagrange multipliers are thus introduced: $\boldsymbol{\lambda}_u \in \mathcal{M}_u$ is devoted to the displacement relation as in the classical approach and $\boldsymbol{\lambda}_\sigma \in \mathcal{M}_\sigma$ is devoted to the constraint (18). The associated new Lagrangian reads:

$$\begin{aligned} L_{\text{new}}\Big((\mathbf{u}_{11},\mathbf{u}_2),(\boldsymbol{\lambda}_u,\boldsymbol{\lambda}_\sigma)\Big) = {} & \frac{1}{2}a_{11}\left(\mathbf{u}_{11},\mathbf{u}_{\mathbf{11}}\right) + \frac{1}{2}a_2\left(\mathbf{u}_2,\mathbf{u}_2\right) - l_{11}\left(\mathbf{u}_{11}\right) - l_2\left(\mathbf{u}_2\right) \\ & + b\left(\boldsymbol{\lambda}_u, \mathbf{u}_{11} - \mathbf{u}_2\right) \\ & + b\left(\boldsymbol{\lambda}_\sigma, \underline{\underline{\sigma_{11}}}(\mathbf{u}_{11})\mathbf{n} - \underline{\underline{\sigma_2}}(\mathbf{u}_2)\mathbf{n}\right), \end{aligned} \tag{19}$$

which enables to get the following variational formulation:

Find $\mathbf{u}_{11} \in \mathcal{U}_{11},\ \mathbf{u}_2 \in \mathcal{U}_2,\ \boldsymbol{\lambda}_u \in \mathcal{M}_u$ and $\boldsymbol{\lambda}_\sigma \in \mathcal{M}_\sigma$ such that:

$$\begin{cases} a_{11}\left(\mathbf{u}_{11}, \mathbf{v}_{11}\right) + b(\boldsymbol{\lambda}_u, \mathbf{v}_{11}) + b(\boldsymbol{\lambda}_\sigma, \underline{\underline{\sigma_{11}}}(\mathbf{u}_{11})\mathbf{n}) = l_{11}\left(\mathbf{v}_{11}\right), \quad \forall \mathbf{v}_{11} \in \mathcal{V}_{11}\ ; \\ a_2\left(\mathbf{u}_2, \mathbf{v}_2\right) - b(\boldsymbol{\lambda}_u, \mathbf{v}_2) - b(\boldsymbol{\lambda}_\sigma, \underline{\underline{\sigma_2}}(\mathbf{u}_2)\mathbf{n}) = l_2\left(\mathbf{v}_2\right), \quad \forall \mathbf{v}_2 \in \mathcal{V}_2\ ; \\ b(\boldsymbol{\mu}_u, \mathbf{u}_{11} - \mathbf{u}_2) = \mathbf{0}, \quad \forall \boldsymbol{\mu}_u \in \mathcal{M}_u\ ; \\ b(\boldsymbol{\mu}_\sigma, \underline{\underline{\sigma_{11}}}(\mathbf{u}_{11})\mathbf{n} - \underline{\underline{\sigma_2}}(\mathbf{u}_2)\mathbf{n}) = 0, \quad \forall \boldsymbol{\mu}_\sigma \in \mathcal{M}_\sigma. \end{cases} \tag{20}$$

This formulation will be denoted "new mortar coupling" in the following of the paper. We will show in section 5 (Numerical results) that the addition of constraint (18) for the coupling enables to represent a C^1 displacement across the interface while only a C^0 solution can be described in the classical approaches. Furthermore, we insist on the fact that the additional constraint considered has a physical meaning from the reference coupling problem. Thus, the new coupling is also suited to describe a solution that is not C^1 across the interface (such as in the case of the coupling of different materials for instance). When the intended solution is not C^1, we will see that no additional errors are introduced since only the interface traction force coming from the discrete displacement is continuous (and not the whole derivative fields of the discrete displacement).

3.2. The discrete version

We now construct the discrete operators associated to the new mortar coupling formulation. To this end, let us introduce the NURBS functions $N_A^{11}, A \in \{1, 2, .., n_{11}\}$ and $N_B^2, B \in \{1, 2, .., n_2\}$ that discretize domains Ω_{11}

and Ω_2, respectively. Following the principle of isoparametric elements, the basis $(N_A^{11})_{A\in\{1,2,..,n_{11}\}}$ and $(N_B^2)_{B\in\{1,2,..,n_2\}}$ are used to build the finite element spaces $\mathcal{U}_{11}^h$ and $\mathcal{U}_2^h$ corresponding to the discretization of $\mathcal{U}_{11}$ and $\mathcal{U}_2$, respectively. As stated above, the discretization of spaces $\mathcal{M}_u$ and $\mathcal{M}_\sigma$ may require special attention to avoid numerical problems. Nevertheless, we have been able to obtain satisfactory results (*i.e.*, that we never encountered instabilities in our computations) with a very basic strategy. For the sake of simplicity, we chose to use the same finite element space $\mathcal{M}^h$ for the two Lagrange multipliers. Then, we adopted a classical strategy (see, *e.g.*, [31]): the trace along the coupling interface Γ of the NURBS functions of subdomain Ω_2 (assumed to be descretized with the finer mesh) was considered for $\mathcal{M}^h$. The resulting one-dimensional functions are denoted $\left(N_D^\lambda\right)_{D\in\{1,2,..,n_\lambda\}}$. We emphasize that other choices could also have been made: for instance, the trace of the NURBS functions of domains Ω_1 along the coupling interface seems to produce equivalent results. By substituting the NURBS approximations in the weak form Eq. (20), we can obtain the following linear system to be solved:

$$\begin{bmatrix} [K_{11}] & [0] & [LA11]^T & [DA11]^T \\ [0] & [K_2] & -[LA2]^T & -[DA2]^T \\ [LA11] & -[LA2] & [0] & [0] \\ [DA11] & -[DA2] & [0] & [0] \end{bmatrix} \begin{Bmatrix} \{U_{11}\} \\ \{U_2\} \\ \{\Lambda_u\} \\ \{\Lambda_\sigma\} \end{Bmatrix} = \begin{Bmatrix} \{F_{11}\} \\ \{F_2\} \\ \{0\} \\ \{0\} \end{Bmatrix}. \tag{21}$$

Operators $[K_{11}]$ (respectively $\{F_{11}\}$) and $[K_2]$ (resp. $\{F_2\}$) are the classical stiffness matrices (resp. vector forces) associated to domains Ω_{11} and Ω_2. $[LA11]$ and $[LA2]$ are the classical mortar coupling operators. $[DA11]$ and

$[DA2]$ are the new mortar coupling operators that enable to enforce the equilibrium of the tractions coming from the discrete displacement along Γ. They are constructed as follows:

$$[LA11] = \int_\Gamma [N_\lambda]^T [nn] \ [D_{11}] \ [B_{11}] \, \mathrm{d}\Gamma \ ; \ \ [LA2] = \int_\Gamma [N_\lambda]^T [nn] \ [D_2] \ [B_2] \, \mathrm{d}\Gamma. \tag{22}$$

$[B_{11}]$ and $[B_2]$ are the standard strain-displacement matrices associated to spaces $\mathcal{U}_{11}^h$ and $\mathcal{U}_2^h$, $[N_\lambda]$ represents the standard shape function matrix of $\mathcal{M}^h$ and $[D_{11}]$ and $[D_2]$ constitute the discrete Hooke matrices. In addition, matrix $[nn]$ is introduced to perform the product between the stress tensor and the outward unit normal (see [9, 26] for more details regarding the construction of such operators).

Remark 5. *Unlike the classical mortar approach, each of the two Lagrange multipliers alone does not have a physical meaning in the proposed formulation. Nevertheless, there exists a combination of the two Lagrange multipliers that can be interpreted as the reaction forces between the two subdomains. Indeed, considering for instance the first set of equations of system* (21)*, we notice that the reaction forces* $\{R_{11}\}$ *along* Γ *of subdomain* Ω_{11} *can be expressed as follows:*

$$\{R_{11}\} = ([K_{11}] \ \{U_{11}\} - \{F_{11}\}) = -[LA1]^T \{\Lambda_u\} - [DA1]^T \{\Lambda_\sigma\}. \tag{23}$$

Remark 6. *Even if presented in the case of elastic constitutive laws, one may notice that the proposed coupling formulation holds for material nonlinearities (such as elastoplasticity). Only additional implementation efforts*

may be taken in this case due to the necessity of evaluating the discrete stress tensor along the coupling interface.

4. Application: development of the non-intrusive coupling strategy

The coupling method developed above can be applied to any NURBS domain decomposition problems (provided higher-order continuity is available at the interface). As an application, we build in this section a non-intrusive algorithm to perform the local enrichment of a NURBS patch with the new mortar coupling. The performance of a non-intrusive strategy for the modeling of local behaviors in a NURBS patch has been demonstrated in Bouclier *et al.* [32]. The goal here is to combine the advantages of a non-intrusive strategy with the property of higher-order continuity of the newly-developed mortar coupling. Since the proposed coupling formulation is based on the use of Lagrange multipliers, the derivation of a non-intrusive strategy is rather straightforward. It is presented briefly in the following. For further details regarding the non-intrusive strategy, we encourage the interested reader to consult [32] and references cited therein.

4.1. The reference non-intrusive global/local problem

In this part, we consider that subdomain Ω_2 represents a local region where a refined model is required to correctly describe the local behavior of the NURBS patch. In the remaining zone of the NURBS patch (*i.e.*, in Ω_{11}), we assume that a coarser and simpler model is sufficient to represent the global behavior of the solution. Rather than solving the system of equations (21) directly (*i.e.*, in a monolithic way), we proceed in an iterative way by involving a global model defined over the existing whole NURBS patch.

The situation is illustrated in Fig. 3. In order to do so, domain Ω_{12} is introduced to characterize the region in which the global model of Ω_{11} is fictively prolonged. Ω_{12} is defined in such a way that the NURBS patch domain is recovered with $\Omega_{11} \cup \Omega_{12}$. From here on, we refer to domain $\Omega_1 = \Omega_{11} \cup \Omega_{12}$ to characterize the global NURBS patch that contains the global model everywhere. The objective of the non-intrusive strategy is then to replace the global model over Ω_{12} by the local one in Ω_2 without actually modifying the global NURBS patch operators over Ω_1.

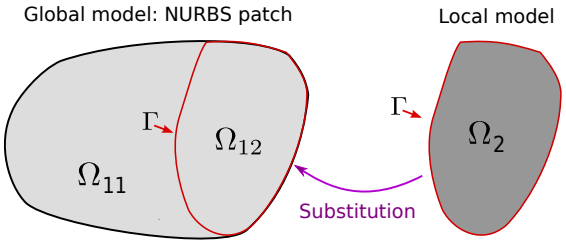

Figure 3: The non-intrusive global/local problem.

4.2. The non-intrusive global/local algorithm

Let us start by introducing the NURBS functions $N^1_C, C \in \{1, 2, .., n_1\}$ that discretize domain Ω_1. As a consequence, the basis functions $(N^{11}_B)_{B\in\{1,2,..,n_{11}\}}$ constitute the restricted part of the basis $(N^1_C)_{C\in\{1,2,..,n_1\}}$ to domain Ω_{11}. To derive the non-intrusive strategy, we perform a continuous prolongation of the displacement solution from Ω_{11} to Ω_{12}. We present the method in the discrete case in the following.

We define $\{U_1\}$ the fictitious prolongation of $\{U_{11}\}$ to Ω_1, so that $\{U_1\}\,|_{\Omega_{11}} = \{U_{11}\}$. The prolonged part of the global solution $\{U_1\}$ to Ω_{12} is denoted

$\{U_{12}\}$ (*i.e.*, $\{U_1\}|_{\Omega_{12}} = \{U_{12}\}$). As well, we introduce the load vector $\{F_1\} = \{F_{11}\} + \{F_{12}\}$ defined on Ω_1. $\{F_{12}\}$ is constructed from body force $\mathbf{f}_{12}^{\mathbf{g}}$ and surface traction $\mathbf{F}_{12}^{\mathbf{g}}$ that can be viewed as the fictitious prolongation of $\mathbf{f}_{11}^{\mathbf{g}}$ and $\mathbf{F}_{11}^{\mathbf{g}}$ to Ω_{12}. In practice, we take $\mathbf{f}_{12}^{\mathbf{g}} = \mathbf{f}_{2}^{\mathbf{g}}$ and $\mathbf{F}_{12}^{\mathbf{g}} = \mathbf{F}_{2}^{\mathbf{g}}$. Then, we make use of the additivity of the integral with respect to domain $\Omega_1 = \Omega_{11} \cup \Omega_{12}$, which gives us:

$$[K_1]\{U_1\} = [K_{11}]\{U_1\} + [K_{12}]\{U_1\}. \tag{24}$$

$[K_1]$ and $[K_{12}]$ are the classical stiffness operators related to domains Ω_1 and Ω_{12}. The equality (24) is used to modify the first part of the equations (21). More precisely, this offers the possibility to split Eq. (21) into two parts: one for each domain Ω_1 and Ω_2. The solution of the coupled problem is finally obtained through an iterative algorithm where the global and local models are computed alternatively. A standard fixed point can be implemented for that. For the n^{th} iteration, we proceed as follows: starting with $\{U_1\}^{(0)}$, $\{\Lambda_u\}^{(0)}$ and $\{\Lambda_\sigma\}^{(0)}$, we look for $\{U_1\}^{(n)}$, $\{U_2\}^{(n)}$, $\{\Lambda_u\}^{(n)}$ and $\{\Lambda_\sigma\}^{(n)}$ such that:

1. Resolution of the full global problem:

$$[K_1]\{U_1\}^{(n)} = \{F_1\} - [LA1]^T\{\Lambda_u\}^{(n-1)} - [DA1]^T\{\Lambda_\sigma\}^{(n-1)} + [K_{12}]\{U_1\}^{(n-1)}. \tag{25}$$

2. Resolution of the local problem:

$$\begin{bmatrix} [K_2] & -[LA2]^T & -[DA2]^T \\ -[LA2] & [0] & [0] \\ -[DA2] & [0] & [0] \end{bmatrix} \begin{Bmatrix} \{U_2\}^{(n)} \\ \{\Lambda_u\}^{(n)} \\ \{\Lambda_\sigma\}^{(n)} \end{Bmatrix} = \begin{Bmatrix} \{F_2\} \\ -[LA1] \ \{U_1\}^{(n)} \\ -[DA1] \ \{U_1\}^{(n)} \end{Bmatrix}. \tag{26}$$

Thanks to the prolongation of the global model over Ω_{12}, the whole stiffness matrix of the global NURBS patch is now considered without any modification. During the iterations, only displacement and force exchanges at the interface Γ are required. In this sense, the strategy is said to be non-intrusive. In our case of a NURBS discretization, this may highly facilitate the modeling of local behaviors since it avoids the complex task of constructing a new NURBS parametrization of the global/local model (and of re-constructing it each time the local region evolves). In addition, it has to be noted that, regardless of the evolution of the shape of the local region, the global stiffness operator is assembled and factorized only once and the system (25) remains well-conditioned. The price to pay is the number of iterations but this one can be deeply reduced by means of accelerations techniques, such as based on an Aitken's Delta Squared method or a Quasi-Newton method (see, *e.g.*, [31, 32]). Numerical experiments to account for this last point will be carried out in section 5 (Numerical results).

Regarding the implementation, the convergence test usually used to stop this algorithm relies on the discrete reaction equilibrium between the two domains. In our case, the global reaction forces along Γ are defined as $\{R_{11}\} = ([K_{11}] \ \{U_{11}\} - \{F_{11}\})|_\Gamma$ and have to be compared to the local reaction forces pulled back in Ω_{11}, *i.e.*: $\{R_2\} = [LA1]^T \{\Lambda_u\} + [DA1]^T \{\Lambda_\sigma\}$.

It leads to the following definition of the interface equilibrium residual:

$$\eta = \frac{|| \{R_{11}\} + \{R_2\} ||}{\sqrt{|| \{F_{11}\} ||^2 + || \{F_2\} ||^2}}. \tag{27}$$

Remark 7. *It may be emphasized that we need to compute the reaction forces over* Γ *of the fictitious part of the global model (*i.e., $[K_{12}]\{U_1\}$*) to make the algorithm work. In order to do so, we use the simple strategy proposed in [32]: the quadrature rule coming from the local problem is transposed within the global NURBS patch to estimate* $[K_{12}]$*. We note that more sophisticated strategies such as the ones elaborated for trimmed surfaces could have been used here (see,* e.g.*, [43, 44, 45]). In the same idea, we need also to compute* $\{R_{11}\}$ *(involving* $[K_{11}]$*) for the interface equilibrium residual* (27)*. The calculation is performed from the already computed stiffness* $[K_{12}]$*,* i.e.*:* $[K_{11}] = [K_1] - [K_{12}]$*.*

Remark 8. *It may also be noted that the fictitious prolongation of the global solution over* Ω_{12} *(*i.e.*,* $\{U_{12}\}$*) has no physical meaning (it depends on the initialization) and has to be replaced by the solution* $\{U_2\}$*.*

5. Numerical examples

To assess the performance of the developed method, four numerical examples are presented in this section. For each, a two-dimensional elastic model under plane stress is considered. The first two test cases are devoted to the study of the new coupling method presented in section 3 without the non-intrusive aspect: the resolution is performed in a monolithic way (*i.e.*, the system of equations (21) is assembled and solved directly). In the

last two numerical problems, the iterative algorithm (25)-(26) of section 4 is implemented in view of performing the non-intrusive local enrichment of a NURBS patch. Unless otherwise stated, we consider quadratic NURBS basis functions with the maximum available continuity at the interior knots (*i.e.* C^1). From here on, the mesh composed of N elements along the first length and M elements along the second length will be denoted $N \times M$.

5.1. Beam under shear load

5.1.1. Presentation and preliminary results.

The first example consists of a beam whose geometry and boundary conditions are given in Fig. 4. This problem has become popular in NURBS to evaluate a coupling method (see, *e.g.*, [9, 24, 26]). The shear load at the right side is parabolic. As a result of the equilibrium of the structure, shear tractions of opposite signs and linearly varying normal tractions are found at the other side. A reference analytical solution is available for the problem in Zienckewich and Taylor [46]. For the coupling, we consider the situation of Fig. 4. The interface Γ is located at the middle of the structure. On this test case, we use the strategies illustrated in Figs. 2(a) and 2(b) to construct different matching and non-matching NURBS discretizations of the domain decomposition problem. We recall that this leads to basis functions of higher-order continuity at the interface Γ. A set of numerical experiments are carried out along with comparisons with classical published NURBS techniques on this test case to show the properties of the proposed coupling approach.

To start with, we plot in Fig. 5 the numerical solution in terms of displacement and von Mises stress for a two non-matching meshes model composed of 5 (along the x-direction) $\times 3$ (along the y-direction) elements in Ω_{11} and

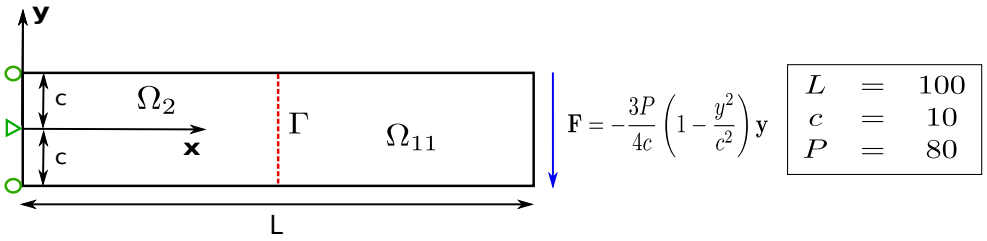

Figure 4: 2D solid beam under shear load: description and data of the problem.

5×5 elements in Ω_2. We consider Young moduli $E_{11} = E_2 = 1000$ and Poisson coefficients $\nu_{11} = \nu_2 = 0.3$. The solution appears to be in a good agreement with references [9, 26]. In particular, the transition of the solution from one model to the other appears very smooth.

(a) Displacement field (magnitude).

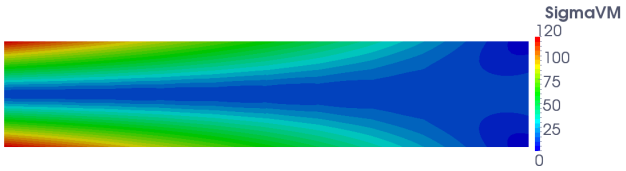

(b) Von Mises stress.

Figure 5: Solution obtained with the new mortar coupling for a two non-matching meshes model (5×3 and 5×5 knot-span elements in Ω_{11} and Ω_2, respectively).

5.1.2. Coupling of matching meshes.

To go further, we investigate more in details the transition across Γ of the component σ_{xx} of the stress tensor. Note that σ_{xx} is also the first component of the traction force that has to be continuous from one model to the other

across the coupling interface Γ according to Eq. (6). First, a two matching meshes model composed of 5×4 elements in Ω_{11} and 5×4 elements in Ω_2 is computed in Figs. 6 and 7. Here, we keep Young moduli $E_{11} = E_2 = 1000$ and Poisson coefficients $\nu_{11} = \nu_2 = 0.3$. More precisely, the distribution of the exact error of the finite element model stress component $\sigma_{xx_{fe}}$, *i.e.* the error with respect to the reference analytical solution $\sigma_{xx_{ex}}$ provided in [46]:

$$\text{Err\_Sig\_xx} = |\sigma_{xx_{fe}} - \sigma_{xx_{ex}}|, \tag{28}$$

is mapped around the interface in Fig. 6 (zoomed window: $L/4 \leq x \leq 3L/4$ and $-c \leq y \leq c$). To better observe the behavior at the interface, the jump of σ_{xx} across Γ with respect to the vertical coordinate y is then plotted in Fig. 7. For comparison purpose, the solutions provided by the basic mortar and basic Nitsche couplings are also computed and added to the graphs. For the Nitsche coupling, the stability factor was set to 20 as in [26]. Finally, reference C^1 and C^0 solutions are added to Fig. 6. The reference C^1 solution is the solution obtained by using a single quadratic C^1 NURBS patch composed of 10×4 knot-span elements for the whole structure (associated knot vector such that $\{0\ 0\ 0\ 0.1\ 0.2\ \ldots\ 0.5\ \ldots\ 0.9\ 1\ 1\ 1\}$ for the x-direction). For the reference C^0 solution, the multiplicity of the middle knot along $\mathbf{x}$ is increased in order to get a C^0 continuity at the interface Γ (knot vector $\{0\ 0\ 0\ 0.1\ 0.2\ \ldots\ 0.5\ 0.5\ \ldots\ 0.9\ 1\ 1\ 1\}$ for the x-direction).

We clearly observe that only the new mortar coupling is able to correctly represent the solution around the interface (see Fig. 6(a)). The error seems to vanish around the interface in this situation. For the classical couplings, error concentrations appear around the interface (see Figs. 6(b) and 6(c)).

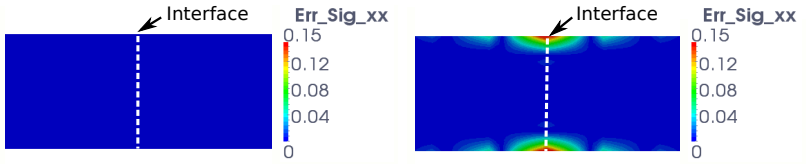

(a) New mortar coupling.

(b) Basic mortar coupling.

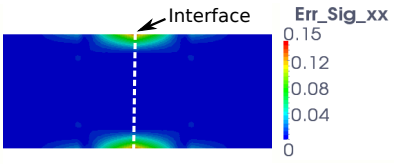

(c) Basic Nitsche coupling.

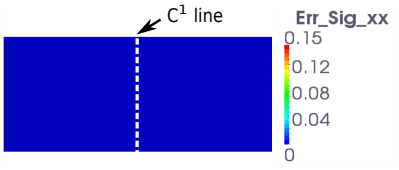

(d) Reference C^1 solution.

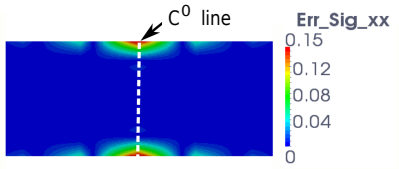

(e) Reference C^0 solution.

Figure 6: Distribution around the coupling interface of the exact error of the stress component σ_{xx} for a two matching meshes model (4×5 knot-span elements in Ω_{11} and Ω_2) and comparison with reference C^1 and C^0 solutions.

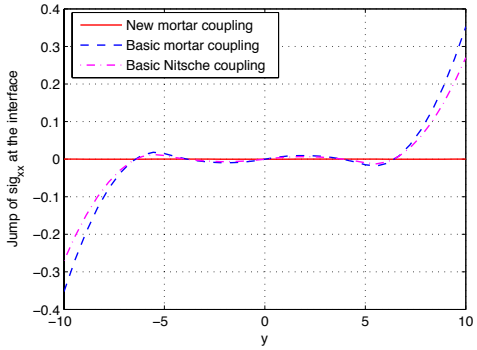

Figure 7: Jump of σ_{xx} along the coupling interface for the two matching meshes model.

By comparing the coupling solutions to the reference C^1 and C^0 solutions (Figs. 6(d) and 6(e)), we notice that a C^1 behavior across the interface can be captured with the new mortar coupling while only a C^0 solution at the interface can be described in the classical approaches. Even if it is only observable for σ_{xx} in the presented figures, we emphasize that exactly the same solutions (in terms of displacements, strains and stresses) are obtained for the new mortar coupling (Fig. 6(a)) as for the equivalent single C^1 patch (Fig. 6(d)). In this sense, our method can be classified as a C^1 coupling method: the whole derivative fields of the coupled solution are continuous across the interface. In the same idea, we can see in Fig. 7 that the jump across Γ of σ_{xx} is null here with the new coupling whereas it increases at the exterior boundaries for the usual coupling techniques. Such a result accounts for the necessity of matching the interface tractions coming from the discrete displacement to get a better transition of the information and so, to obtain a better accuracy of the coupled solution.

5.1.3. Coupling at a bi-material interface.

To assess the performance of the proposed coupling method in situations where the solution is not C^1 across the interface, the same numerical experiment as in the previous section is carried out but with different constitutive materials for the subdomains. More precisely, we take $E_{11} = 500$ in Ω_{11} and $E_2 = 1000$ in Ω_2 (and $\nu_{11} = \nu_2 = 0.3$). Since the problem is isostatic, the same reference solution in terms of stress as for the problem in [46] should be reached. Fig. 8 shows the distribution of the exact error of σ_{xx} around the coupling interface. As in the previous part, the results of the new mortar coupling along with the classical couplings are given and reference C^1 and

C^0 solutions are also added. For the reference solutions, exactly the same parametrizations as previously are taken but this time, $E_{11} = 500$ is applied on the right part of the patch and $E_2 = 1000$ is applied in the remaining left area. For completeness, the evolution of the exact error regarding σ_{xx} at each side of the interface with respect to the vertical coordinate y is plotted in Fig. 9. The jump of σ_{xx} across the coupling interface is not plotted for this numerical experimentation since it can be observed in Fig. 9 with the discrepancy between the left and right interface errors.

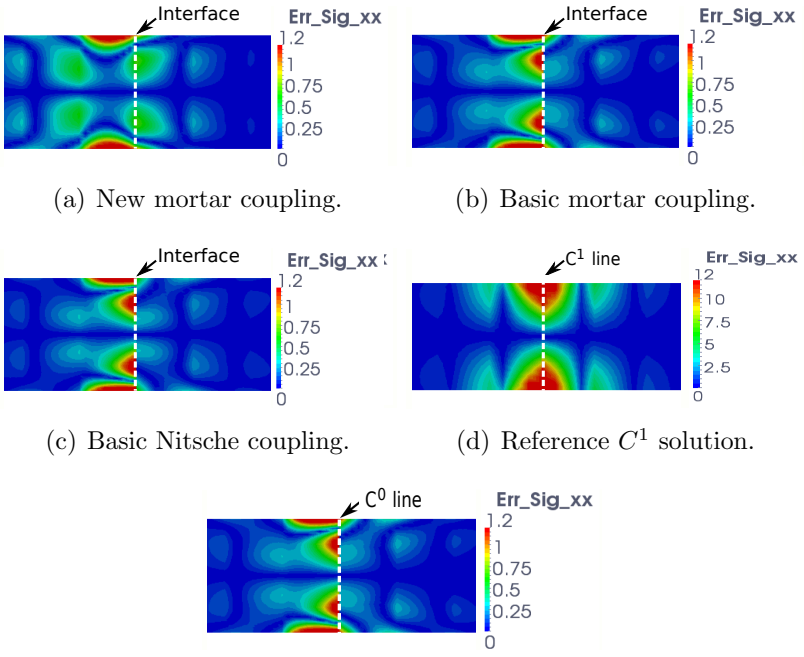

(a) New mortar coupling. (b) Basic mortar coupling.

(c) Basic Nitsche coupling. (d) Reference C^1 solution.

(e) Reference C^0 solution.

Figure 8: Distribution around the coupling interface of the exact error of the stress component σ_{xx} for the modeling of a bi-material structure with matching meshes (5×4 knot-span elements in Ω_{11} and Ω_2) and comparison with reference C^1 and C^0 solutions.

This time, the reference C^1 solution (Fig. 8(d)) does not allow for a cor-

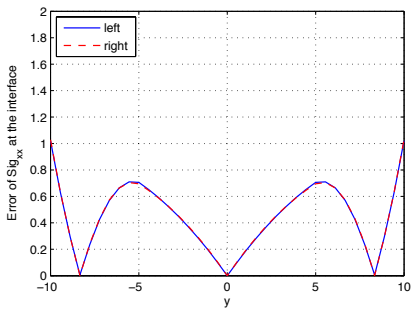

(a) New mortar coupling.

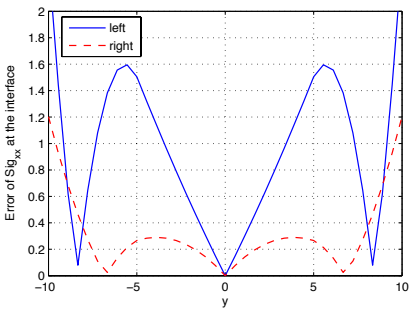

(b) Basic mortar coupling.

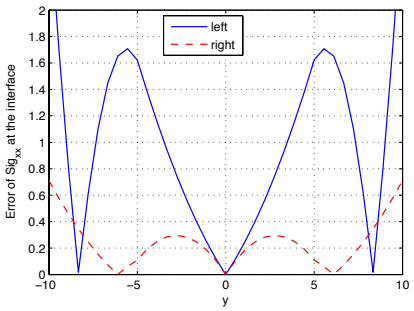

(c) Basic Nitsche coupling.

Figure 9: Evolution of the exact error of σ_{xx} along the coupling interface for the modeling of a bi-material structure with matching meshes.

rect representation of the behavior at the interface (note that the error scale is multiplied by a factor of ten in contrast to the other solutions). Such a behavior was expected here since the whole derivative fields (*i.e.*, all the strain and stress components) are C^0 at the interface for a C^1 solution, which is meaningless from a physical point of view. On the contrary, putting a C^0 line at the interface enables to significantly reduce the error (see Fig. 8(e)). As before, we observe that the classical coupling approaches (Figs. 8(b) and 8(c)) are able to represent a C^0 solution at the interface. Now, what is interesting to observe here is that our proposed coupling approach seems to be efficient as well to address bi-material interfaces (see Fig. 8(a)). This is due to the fact that the quantities that are transmitted from one model to the other (the discrete displacement and the traction coming from the discrete displacement) are consistent with the initial mechanical problem. In the new coupling solution (Fig. (8(a))), only these quantities are continuous but not the whole derivatives as in the reference C^1 solution. We therefore end up with a coupled solution that is meaningful at a physical point of view, and that enables a better transition of the information at the coupling interface, which leads to a global diminution of the coupling error (see Fig. (9)).

5.1.4. Coupling of non-matching meshes.

The coupling of non-matching NURBS meshes is now investigated. For that, the problem of Fig. 4 is computed again with $E_{11} = E_2 = 1000$ for a two non-matching meshes model composed of 5×3 elements in Ω_{11} and 5×5 elements in Ω_2. The distribution of the exact error of σ_{xx} around the coupling interface is shown in Fig. 10. The evolution of the exact error at each side of the interface with respect to the vertical coordinate y is also

plotted in Fig. 11 before showing the stress jump across Γ in Fig. 12.

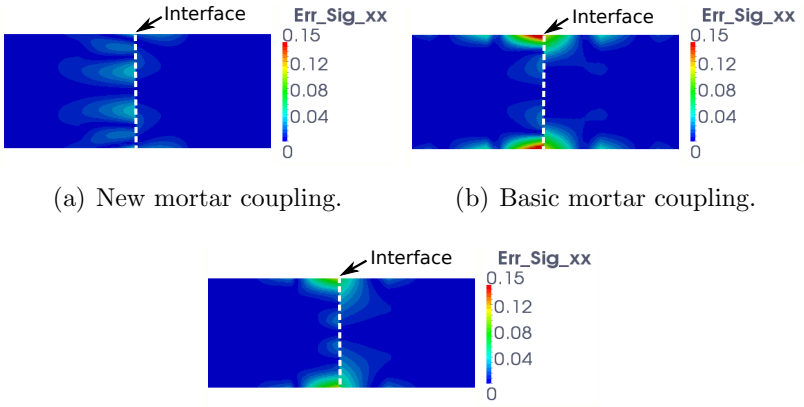

(a) New mortar coupling. (b) Basic mortar coupling.

(c) Basic Nitsche coupling.

Figure 10: Distribution around the coupling interface of the exact error of the stress component σ_{xx} for a two non-matching meshes model (5×3 knot-span elements in Ω_{11} and 5×5 in Ω_2).

Some error concentrations can be observed at the coupling interface for every method due to the use of non-matching meshes. Once again, it appears that the proposed method results in lower error concentrations (particularly at the exterior boundaries) due to lower stress jumps at the coupling interface.

5.1.5. Convergence behavior in strain energy.

As it has been done for classical mortar and Nitsche couplings (see, *e.g.*, [9, 26, 23]), we finally check the convergence of the new mortar coupled solution with respect to the refinement of the mesh. In order to do so, we consider again the problem of Fig. 4 (with $E_{11} = E_2 = 1000$) and we proceed as in [46]: the convergence behavior in strain energy is studied. The relative

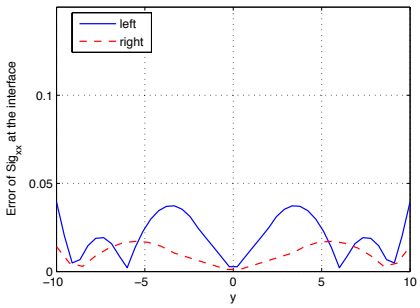

(a) New mortar coupling.

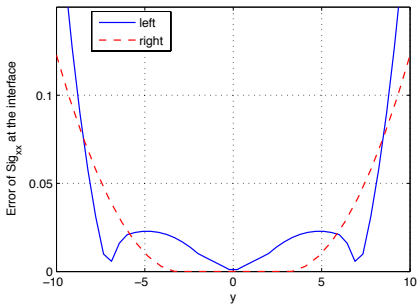

(b) Basic mortar coupling.

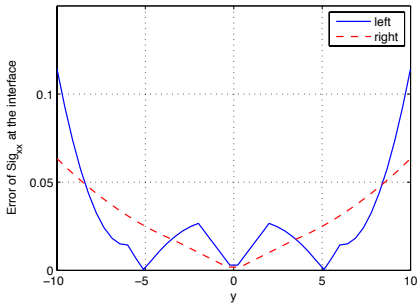

(c) Basic Nitsche coupling.

Figure 11: Evolution of the exact error of σ_{xx} along the coupling interface for the two non-matching meshes model.

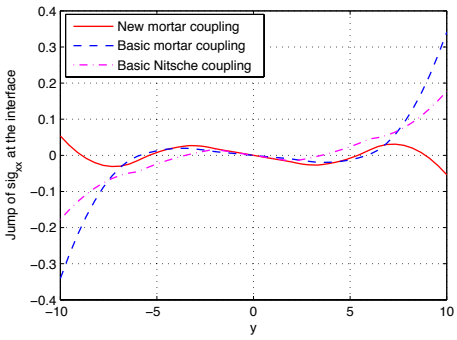

Figure 12: Jump of σ_{xx} along the coupling interface for the two non-matching meshes model.

energy error is computed as:

$$\frac{|E_{ex} - E_{fe}|}{E_{ex}}, \tag{29}$$

where E_{fe} denotes the strain energy of the NURBS finite element model and E_{ex} denotes the reference exact strain energy equals to 3296 according to [46]. The coupling of matching and non-matching meshes is investigated. For the refinement, the meshes indicated in Tab. 1 are used. We recall that quadratic NURBS meshes are considered, the continuity at the interior lines (and so, at the interface) being C^1. The convergence curves are finally plotted in Fig. 13 with respect to the equivalent number of elements N^{el} normalized by the number of elements N_1^{el} of the equivalent single-patch coarsest mesh (see left column of Tab. 1 for the associated values).

Number of elements (N^{el})	Single-patch mesh	Two matching meshes ($\Omega_{11} \cup \Omega_2$)	Two non-matching meshes ($\Omega_{11} \cup \Omega_2$)
40 ($= N_1^{el}$)	10×4	$5 \times 4 \cup 5 \times 4$	$5 \times 3 \cup 5 \times 5$
160	20×8	$10 \times 8 \cup 10 \times 8$	$10 \times 6 \cup 10 \times 10$
640	40×16	$20 \times 16 \cup 20 \times 16$	$20 \times 12 \cup 20 \times 20$
2560	80×32	$40 \times 32 \cup 40 \times 32$	$40 \times 24 \cup 40 \times 40$

Table 1: Meshes considered to study the convergence behavior.

We observe that the convergence rate and the error constant of the coupled discretizations are equivalent to the ones of the equivalent single-patch discretization. As emphasized above, the solutions are exactly the same for matching meshes (see Fig. 13(a)). For sure, a slight discrepancy appears for non-matching meshes (see Fig. 13(b)) since in this case the single-patch model cannot exactly represent the coupled model. These convergence curves demonstrate that the developed coupling method does not interfere with the

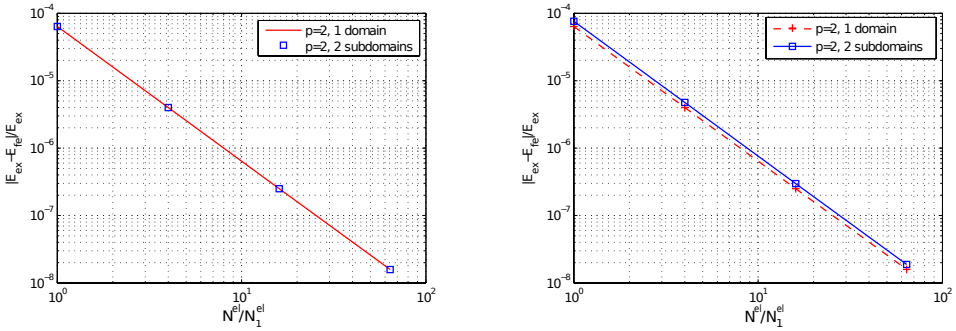

(a) Matching meshes. (b) Non-matching meshes.

Figure 13: Convergence of the strain energy for uniform refinement in both subdomains.

global increased accuracy achieved by the NURBS functions.

5.2. Plate composed of a trimmed B-spline patch and a circular NURBS domain

With the next example, the coupling of non-conforming geometries is investigated (see Fig. 2(c) as a reminder). The test case concerns an homogeneous rectangular plate subjected to constant in-plane tension (see Fig. 14(a)). The geometric model of the plate consists of a quadratic trimmed B-spline patch and a quadratic circular NURBS domain that are connected via a circular NURBS curve (see Fig. 14(b) for illustration). Since the connecting curve is inside the quadratic B-spline patch, the continuity of the basis functions of Ω_{11} along Γ is at least C^1. To build the NURBS circular domain Ω_2, we extract it from a larger quadratic NURBS patch containing an additional layer of two elements (following the strategy depicted in remark 3). In this way, the continuity of the basis functions of Ω_2 is C^1 at the interface Γ. We finally make use of a fictitious domain method to compute the solution on the grey part of the two NURBS entities.

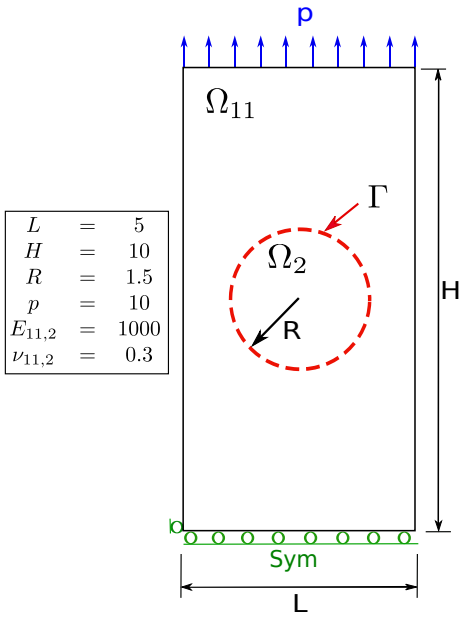

(a) Description and data of the problem.

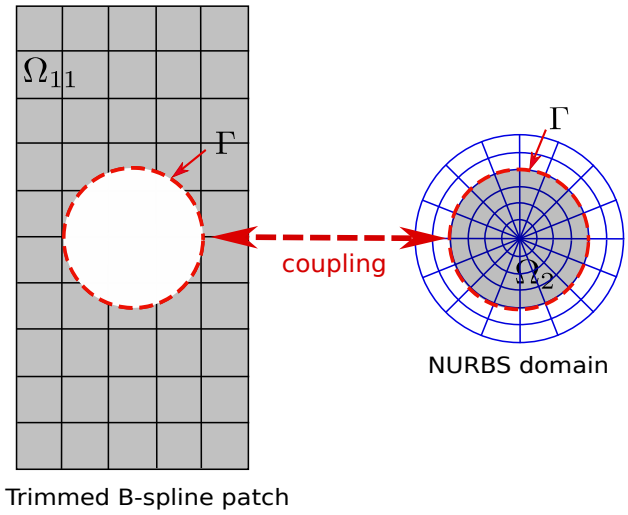

(b) Discretization of the coupling problem.

Figure 14: Plate under uniaxial stress modeled by a trimmed B-spline patch and a circular NURBS domain.

The results in terms of displacement and stress of the two-domain problem using the new mortar and classical mortar couplings are given in Fig. 15. The correct displacement seems to be obtained with the two coupling strategies. However, a discontinuity of the stresses can be observed with the classical mortar coupling which leads to some error concentrations at Γ (see Fig. 15(d), the desired stress being $p = 10$). The discontinuity seems to completely disappear in the new mortar coupling solution, which goes with a diminution of the maximum level of error.

5.3. Non-intrusive analysis of a frame

In the third example, the non-intrusive algorithm (25)-(26) is investigated for the coupling of two non-matching meshes model. A plane frame analysis is performed to this end. The numerical problem considered is taken from Nguyen *et al.* [24] where a reference solution is provided. As an application of the use of the non-intrusive coupling strategy, we propose to illustrate, with this problem, the possibility of making non-intrusive NURBS local refinement.

The numerical model is described in Fig. 16. Due to symmetry, only half of the problem is analysed with appropriate symmetric boundary conditions. For the discretization of the problem, a C^0 line is set up between the two arms since the geometry at this location is C^0. To get a good accuracy, a quadratic NURBS patch composed of 2 elements into the thickness direction has been considered for the global model. Into the length direction, we take 8 elements for the vertical arm and 4 elements for the horizontal one. The local model, located into the corner, is composed of a quadratic mesh of 8 (thickness direction) $\times$4 (length direction) for both the vertical and the

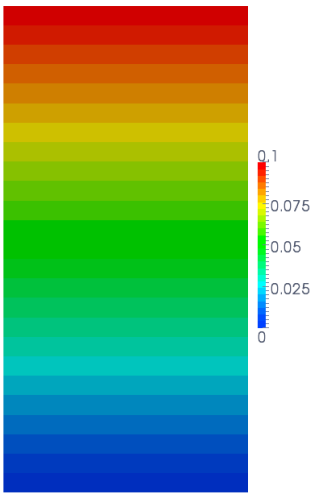

(a) New mortar coupling: disp. $\mathbf{u_y}$.

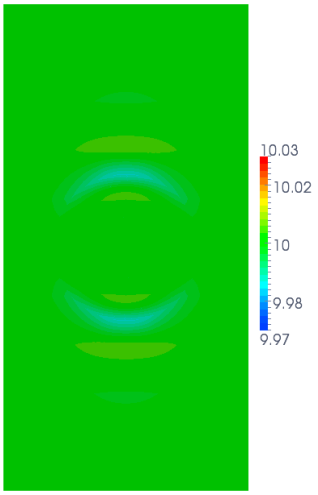

(b) New mortar coupling: VM stress σ_{vm}.

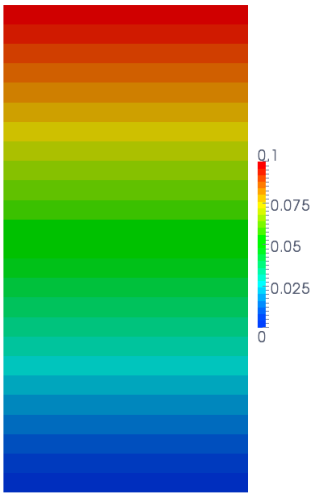

(c) Basic mortar coupling: disp. $\mathbf{u_y}$.

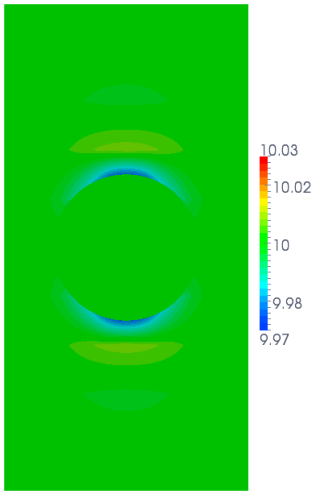

(d) Basic mortar coupling: VM stress σ_{vm}.

Figure 15: Coupled solution for the plate composed of a trimmed B-spline patch and a circular NURBS domain (top: new mortar coupling, bottom: basic mortar coupling).

horizontal arm. The continuity of the functions at the interior lines dividing the patch into elements is C^1 everywhere except at the corner line between the two arms where it is C^0. The aim of the non-intrusive algorithm is to replace the global coarse solution at the corner by a local finer solution thanks to the exchange of interface data only between the two models.

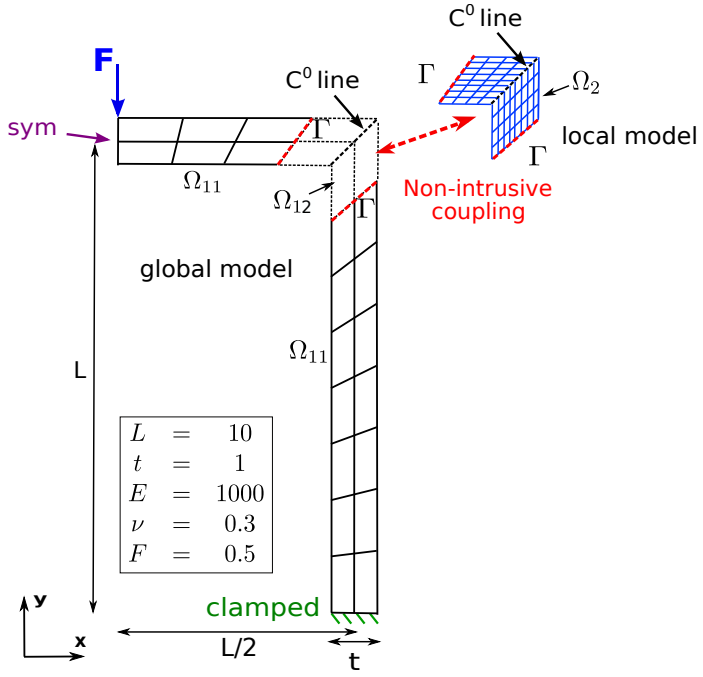

Figure 16: Non-intrusive plane frame analysis: problem description.

The deformed configurations obtained once the non-intrusive algorithm with the new mortar coupling has converged are shown in Fig. 17(a). More precisely, the global solution (with the fictitious prolongation over the local area in the corner) and the local solution are plotted on the left while the combination of the two solutions (the true coupled solution) is represented on the right. As a reference for the refinement, we also compute in Fig. 17(b)

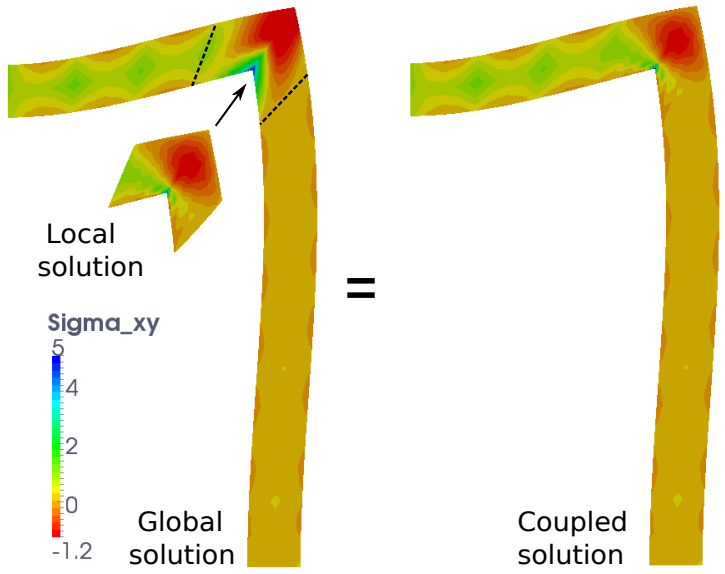

(a) Converged solution of the non-intrusive algorithm with the new mortar coupling.

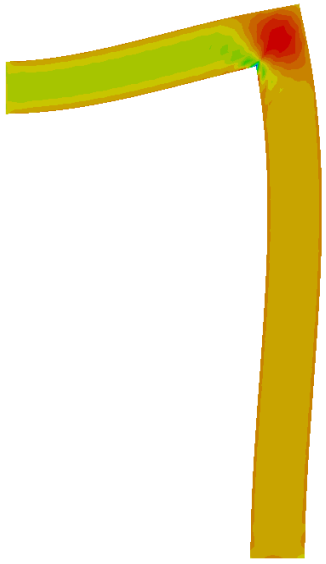

(b) Globally refined solution.

Figure 17: Deformed configuration (scale factor 8) : contour plot of σ_{xy}.

the globally refined model composed of 8×32 elements for the vertical arm and 8×16 elements for the horizontal arm. More precisely, the contour plot of the stress component σ_{xy} is given. The global solution around the corner of the frame has to be replaced by the solution of the local model to correctly represent, in this area, the response of the structure.

In Figs. 18(a) and 18(b), the convergence of the non-intrusive strategy for the new mortar coupling is investigated. The standard fixed point (formed by Eqs. (25) and (26)) is implemented first. Then, the Aitken's Delta squared and Quasi-Newton acceleration techniques are applied to the present situation to reduce the number of iterations. As expected, we observe in Fig. 18(a) that the equilibrium residual (see Eq. (27)) goes down to 0. In Fig. 18(b), the strain energy of the coupled model is plotted during the iterations of the algorithm. For comparison purpose, the strain energy obtained when performing a monolithic resolution of the same coupled problem is added to this figure. We see that the monolithic solution is reached by the converged iterative solution which accounts for the accuracy of the non-intrusive algorithm. Furthermore, we emphasize that the use of acceleration techniques enables to deeply reduce the number of iterations of the algorithm. On our example, a residual below 10^{-3} can be reached in a tenth of iterations with such acceleration techniques (see Fig. 18(a)). From the convergence of the strain energy in Fig. 18(b), it can actually be observed that only 4-5 iterations seem to be necessary to reach the monolithic solution. Regarding NURBS local refinement, the price to pay to get a non-intrusive strategy appears then reasonable compared to an intrusive monolithic resolution. For completeness, we also show the convergence behavior obtained, on the same problem, using

a non-intrusive strategy with the classical mortar coupling (see Figs. 18(c) and 18(d)). An equivalent behavior is observed between the two strategies which means that we do not deteriorate the efficiency of the non-intrusive algorithm with the new mortar coupling.

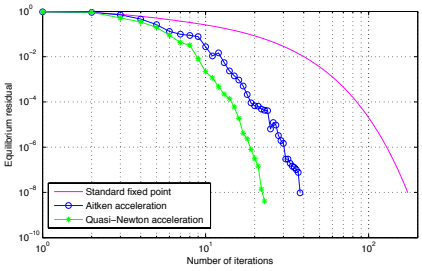

(a) New mortar coupling: Convergence of the interface equilibrium residual.

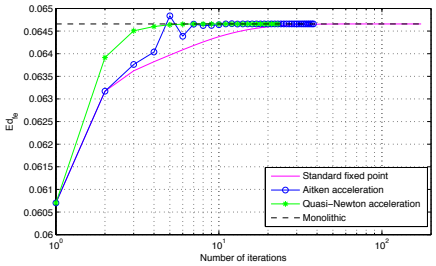

(b) New mortar coupling: Convergence of the strain energy.

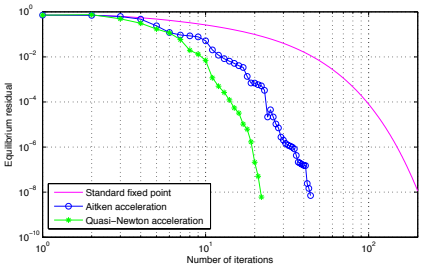

(c) Basic mortar coupling: Convergence of the interface equilibrium residual.

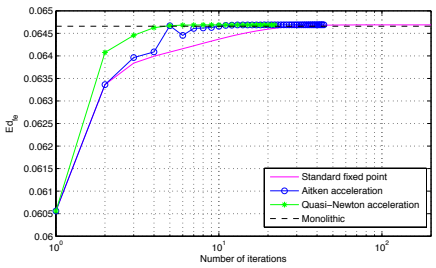

(d) Basic mortar coupling: Convergence of the strain energy.

Figure 18: Convergence of the non-intrusive algorithm (top: new mortar coupling, bottom: basic mortar coupling).

However, the converged solutions differ between the new and classical mortar couplings. A zoomed view of the converged coupled deformed configuration around the top coupling interface has been done in Fig. 19 to highlight the difference. In Fig. 19(a), the new mortar coupling is performed while in Fig. 19(b), the basic mortar coupling is considered. We clearly see an

undesirable discontinuity at the coupling interface with the basic approach whereas the transition of the solution appears sufficiently smooth with the new approach.

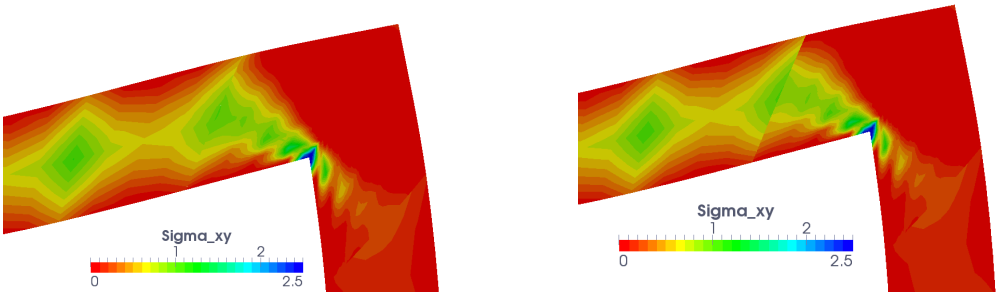

(a) New mortar coupling. (b) Basic mortar coupling.

Figure 19: Comparison between the new mortar coupling solution and the basic mortar coupling solution: zoomed window of plot of σ_{xy} at the top interface of the two meshes.

5.4. Non-intrusive analysis of a plate with a center inclusion

The last numerical example concerns the non-intrusive modeling of a center inclusion within a plate subjected to constant in plane tension (see Fig. 20(a)). So as to be consistent with composite materials, the Young modulus for the inclusion is chosen a hundred times larger than for the plate. One may note that such types of test cases have already been computed using an embedded Nitsche method (see, *e.g.*, [9]), and that exactly the same problem has been investigated in Bouclier *et al.* [32] with the classical mortar non-intrusive approach. Here, we perform the computation with the new mortar non-intrusive algorithm (25)-(26).

Regarding the coupled model, we consider that the local region Ω_2 includes the inclusion along with, on the edge, an annulus of two elements

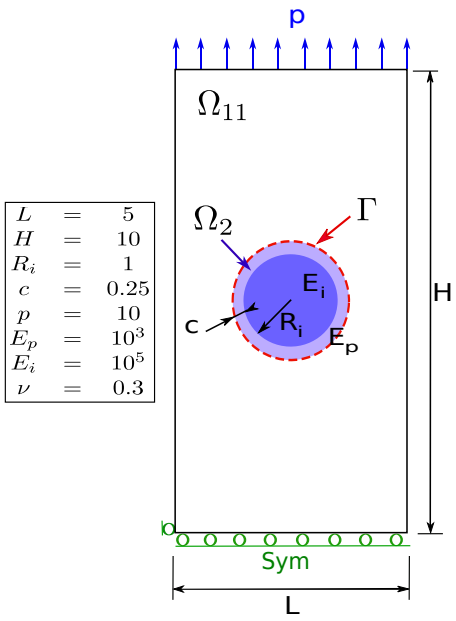

(a) Description and data of the problem.

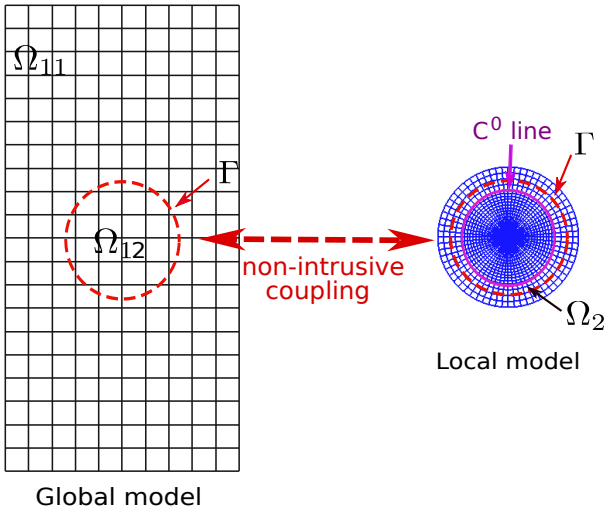

(b) Discretization of the coupling problem.

Figure 20: Non intrusive study of a plate with a center inclusion.

(into the radial direction) whose material behavior is the same as in the plate (see, again, Fig. 20). This means that the same materials near the circular interface Γ are connected in the global/local simulation which allows for a better efficiency of the non-intrusive strategy (see [32] for a detailed account regarding this point). For the sake of simplicity, we put a C^0 line to separate the two materials in the local model (see *magenta* line) but one may note that our new mortar coupling could have been used instead. As in the example 5.2, the local discretization is constructed from a larger quadratic NURBS circular patch to get a C^1 continuity of the local solution at Γ. More precisely, the inclusion is composed of 64 (circumferential direction) $\times$16 (radial direction) elements and a mesh of 64×2 is considered for the annulus. The global model constitutes the whole plate discretized using a 10×20 quadratic B-spline patch.

The results are given in Fig. 21. Figs. 21(a)-21(c) show, respectively, the vertical displacement, the vertical strain and the von Mises stress. The solution is globally in a good agreement with the solution computed in [32]. The stiffer behavior of the inclusion seems to be well captured: the vertical strain is low while the von Mises stress is high in the inclusion. As in [32], a residual below 10^{-3} for the non-intrusive algorithm has been reached in a few tenths of iterations with the Newton acceleration technique on this test case.

To finish, we make a comparison in Fig. 22 with the solution obtained using the classical mortar non-intrusive strategy. The vertical strain is plotted around the interface Γ for the two mortar couplings. Once again, we observe a discontinuity of the strain with the classical mortar solution around the

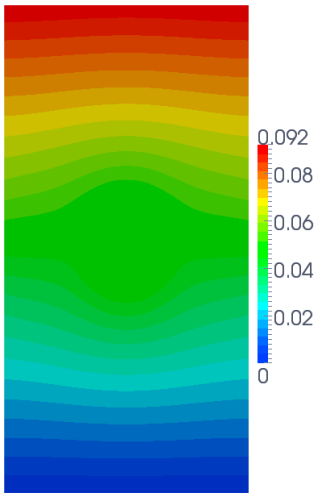

(a) Converged solution: disp. $\mathbf{u_y}$.

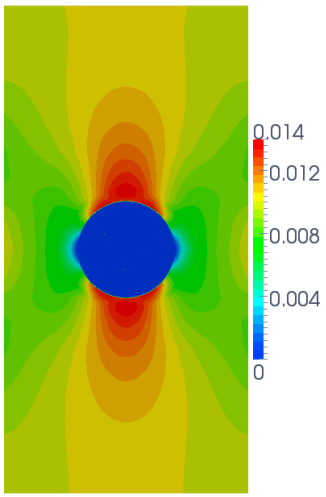

(b) Converged solution: strain ε_{yy}.

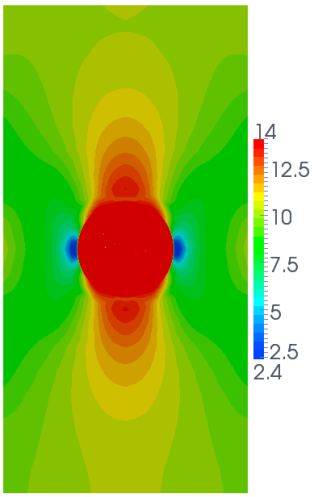

(c) Converged solution: VM stress σ_{vm}.

Figure 21: Non-intrusive analysis with the new mortar coupling of a plate with a center inclusion.

interface Γ at the top and at the bottom (see Fig. 22(b)). In contrast, the solution appears to be perfectly smooth with the new mortar coupling (see Fig. 22(a)). For completeness, the difference between the two solutions (*i.e.*: $|\varepsilon_{yy_{C1}} - \varepsilon_{yy_{C0}}|$ where $\varepsilon_{yy_{C1}}$ and $\varepsilon_{yy_{C0}}$ are the solutions associated the new and classical mortar couplings, respectively) is plotted in Fig. 22(c). Therefore, the proposed coupling method seems to respect the analysis properties of IGA: it enables to get a smoother solution when it is meaningful from a physical point of view.

6. Conclusion

In this paper, we have developed a new coupling method to connect different NURBS subdomains within a NURBS patch. The objective is to address the difficulty of integrating different discrete models in different regions of a NURBS patch. The interest of the developed method is that it makes use of the higher-order continuity offered by the NURBS basis functions. In order to do so, we have proposed to match, across the coupling interface, the traction forces coming from the discrete displacement as well as the usual discrete displacements. Since the two quantities transmitted in the coupling formulation are consistent with respect to the initial mechanical problem, we end up with a strategy that is suitable with the continuity of the physical solution: when the physical solution is sufficiently smooth, the strategy enables to represent a C^1 behavior; but, when only a C^0 displacement is expected (such as in the case of bi-material structures for instance), no additional errors are introduced since only the traction force is continuous and not the whole derivative fields. The performance of the developed method has been

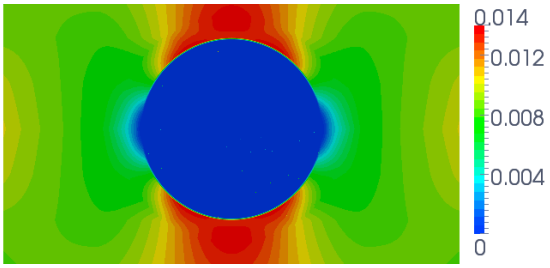

(a) New mortar coupling.

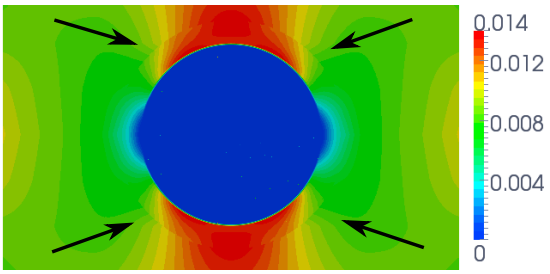

(b) Basic mortar coupling.

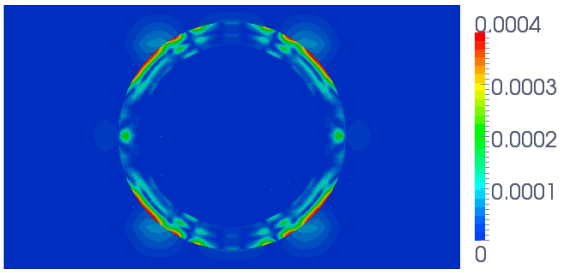

(c) Difference between the two couplings.

Figure 22: Comparison between the new mortar coupling solution and the basic mortar coupling solution: zoomed window of plot of ε_{yy} around the interface.

demonstrated on a set of numerical experiments involving the coupling of matching meshes, non-matching meshes, and non-conforming geometries in 2D linear elasticity. It has been observed that the new coupling method results in lower stress jumps at the coupling interface than the classical NURBS coupling techniques (basic mortar [23, 32] and Nitsche [9, 26, 23]), which allows for a better transition of the mechanical information from one model to the other. The developed approach appears then to us more consistent with the analysis properties of IGA since it allows for a smoother representation of the solution across the interface.

To ensure the two coupling constraints, a Lagrange multiplier approach has been considered. As a consequence, we have introduced two Lagrange multipliers: the first one is devoted to the continuity of the discrete displacement as usual, and the second one enables to ensure the additional constraint, *i.e.*, the continuity of the traction force coming from the discrete displacement. Since based on the use of Lagrange multipliers, we have been able to build a non-intrusive algorithm for the resolution of the new coupling formulation. As demonstrated in [32], a non-intrusive methodology appears well-suited for the local enrichment of NURBS patches. The main advantages are: the elimination of costly NURBS re-parametrization procedures for the global model (even if the local area evolves), the possibility to assemble and factorize the global stiffness operator only once, and the good conditioning of the systems to be solved. Therefore, the combination of a non-intrusive approach with the developed coupling method offers the possibility to simply model local behaviors within a NURBS patch, with the additional benefit of a smoother transition of the solution between the global and local models.

Even if the numerical experiments have been limited to two-dimensional linear elasticity in this work, the proposed coupling method may easily apply to three dimensions and nonlinear models (see, *e.g.*, [31] in the context of standard non-intrusive FEM). This opens the door to tackle more realistic engineering applications. Furthermore, it has to be noted that the non-intrusive local enrichment of NURBS patches may not be the only application of such a method. Indeed, taking advantage of the Lagrange multipliers approach, the proposed methodology seems to be adapted to the development of more regular non-overlapping domain decomposition methods to be used for high performance computing on parallel computer architectures (see, *e.g.*, [38, 39, 40] for the elaboration in the context of classical FEM). In addition, in the same idea of what is performed in [47], such a coupling may also serve as a basis to develop a strategy that could connect different NURBS patches while ensuring a C^1 continuity at the interface. This would enable to construct full C^1 multi-patch geometries.

Acknowledgements

The authors would like to acknowledge the financial support of the French National Research Agency under Grant ICARE ANR-12-MONU-0002.

References

[1] T.J.R. Hughes, J.A. Cottrell, Y. Bazilevs, Isogeometric analysis: CAD, finite elements, NURBS, exact geometry, and mesh refinement, *Computer Methods in Applied Mechanics and Engineering* 194 (2005) 4135-4195.

[2] J.A. Cottrell, T.J.R. Hughes, Y. Bazilevs. Isogeometric analysis: Toward Integration of CAD and FEA, *Wiley* 2009.

[3] J. Evans, Y. Bazilevs, I. Babuska, T.J.R. Hughes, n-widths, sup-infs, and optimality ratios for the k-version of the isogeometric finite element method, *Computer Methods in Applied Mechanics and Engineering* 198 (2009) 1726-1741.

[4] J.A. Cottrell, A. Reali, Y. Bazilevs, T.J.R. Hughes, Isogeometric analysis of structural vibrations, *Computer Methods in Applied Mechanics and Engineering* 195 (2006) 5257-5296.

[5] D. Schillinger, J.A. Evans, A. Reali, M.A. Scott, T.J.R. Hughes, Isogeometric Collocation: Cost Comparison with Galerkin Methods and Extension to Adaptive Hierarchical NURBS Discretizations, *Computer Methods in Applied Mechanics and Engineering* 267 (2013) 170-232.

[6] D. Schillinger, M. Ruess, N. Zander, Y. Bazilevs, A. Düster, E. Rank, Small and large deformation analysis with the $p-$ and B-spline versions of the Finite Cell Method, *Computational Mechanics* 50 (2012) 445-478.

[7] R. Echter, M. Bischoff, Numerical efficiency, locking and unlocking of NURBS finite elements, *Computer Methods in Applied Mechanics and Engineering* 199 (2010), 374-382.

[8] R. Bouclier, T. Elguedj, A. Combescure, An isogeometric locking-free NURBS-based solid-shell element for geometrically nonlinear analysis, *International Journal for Numerical Methods in Engineering* 101 (2015) 774-808.

[9] V.P. Nguyen, P. Kerfriden, M. Brino, S.P.A. Bordas, E. Bonisoli, Nitsche's method for two and three dimensional NURBS patch coupling, *Computational Mechanics* 53 (2014) 1163-1182.

[10] C.A. Duarte, D.J. Kim, Analysis and applications of a generalized finite element method with global-local enrichment functions, *Computer Methods in Applied Mechanics and Engineering* 197 (2008) 487-504.

[11] J.C. Passieux, J. Réthoré, A. Gravouil, M.C. Baietto, Local/global non-intrusive crack propagation simulation using multigrid XFEM solver, *Computational Mechanics* 52 (2013) 1381-1393.

[12] L. Gendre, O. Allix, P. Gosselet, F. Comte, Non-intrusive and exact global/local techniques for structural problems with local plasticity, *Computational Mechanics* 44 (2009) 233-245.

[13] C. Rabut, Locally tensor product functions, *Numerical Algorithms* 39 (2005) 329-348.

[14] A.V. Vuong, C. Giannelli, B. Juttler, B. Simeon, A hierarchical approach to adaptive local refinement in isogeometric analysis, *Computer Methods in Applied Mechanics and Engineering* 200 (2011) 3554-3567.

[15] D. Schillinger, L. Dede, M.A. Scott, J.A. Evans, M.J. Borden, E. Rank, T.J.R. Hughes, An isogeometric design-through-analysis methodology based on adaptive hierarchical refinement of NURBS, immersed boundary methods, and T-spline CAD surfaces, *Computer Methods in Applied Mechanics and Engineering* 249-252 (2012) 116-150.

[16] T. Dokken, T. Lyche, K.F. Pettersen, Polynomial splines over locally refined box-partitions, *Computer Aided Geometric Design* 30 (2013) 331-356.

[17] Y. Bazilevs, V.M. Calo, J.A. Cottrell, J.A. Evans, T.J.R Hughes, S. Lipton, Isogeometric analysis using T-splines. *Computer Methods in Applied Mechanics and Engineering* 199 (2010) 229-263.

[18] M.A. Scott, X. Li, T.W. Sederberg, T.J.R. Hughes, Local refinement of analysis-suitable T-splines, *Computer Methods in Applied Mechanics and Engineering* 213-216 (2012) 206-22.

[19] L. Beirão da Veiga, A. Buffa, D. Cho, G. Sangalli, Analysis-suitable T-splines are dual-compatible, *Computer Methods in Applied Mechanics and Engineering* 249 (2012) 42-51.

[20] A. Chemin, T. Elguedj, A. Gravouil, Isogeometric local h-refinement strategy based on multigrids, *Finite Elements in Analysis and Design* 100 (2017) 77-90.

[21] C. Hesch, P. Betsch, Isogeometric analysis and domain decomposition methods, *Computer Methods in Applied Mechanics and Engineering* 213-216 (2012) 104-112.

[22] E. Brivadis, A. Buffa, B. Wohlmuth, L. Wunderlich, Isogeometric Mortar methods, *Computer Methods in Applied Mechanics and Engineering* 284 (2015) 292-319.

[23] A. Apostolatos, R. Schmidt, R. Wuchner, K.U. Bletzinger, A Nitsche-type formulation and comparison of the most common domain decom-

position methods in isogeometric analysis, *International Journal for Numerical Methods in Engineering* 97 (2014) 473-504.

[24] V.P. Nguyen, P. Kerfriden, S. Claus, S.P.A. Bordas, Nitsche's method method for mixed dimensional analysis: conforming and non-conforming continuum-beam and continuum-plate coupling, arXiv:1308.2910v1.

[25] Y. Guo, M. Ruess, Nitsche's method for a coupling of isogeometric thin shells and blended shell structures, *Computer Methods in Applied Mechanics and Engineering* 284 (2015) 881-905.

[26] M. Ruess, D. Schillinger, A.I. Özcan, E. Rank, Weak coupling for isogeometric analysis of non-matching and trimmed multi-patch geometries, *Computer Methods in Applied Mechanics and Engineering* 269 (2014) 46-71.

[27] W. Dornisch, G. Vitucci, S. Klinkel, The weak substitution method – An application of the mortar method for patch coupling in NURBS-based isogeometric analysis, *International Journal for Numerical Methods in Engineering* 103 (2015) 205–234.

[28] J.D. Whitcomb, Iterative global/local finite element analysis, *Computers & Structures*, 40 (1991) 1027-1031.

[29] M. Chevreuil, A. Nouy, E. Safatly, A multiscale method with patch for the solution of stochastic partial differential equations with localized uncertainties, *Computer Methods in Applied Mechanics and Engineering* 255 (2013) 255-274.

[30] G. Guguin, O. Allix, P. Gosselet, S. Guinard, Nonintrusive coupling of 3D and 2D laminated composite models based on finite element 3D recovery, *International Journal for Numerical Methods in Engineering* 98 (2014) 324-343.

[31] M. Duval, J.C. Passieux, M. Salaün, S. Guinard, Non-intrusive coupling: recent advances and scalable nonlinear domain decomposition, *Archives of Computational Methods in Engineering* 23 (2016) 17-38.

[32] R. Bouclier, J.-C. Passieux and M. Salaün, Local enrichment of NURBS patches using a non-intrusive coupling strategy: geometric details, local refinement, inclusion, fracture, *Computer Methods in Applied Mechanics and Engineering* 300 (2016) 1-26.

[33] E. Cohen, T. Lyche, R. Riesenfeld, Discrete B-spline and subdivision techniques in computer aided geometric design and computer graphics, *Computer Graphics and Image Processing*, 14 (1980) 87-111.

[34] L. Piegl, W. Tiller, The NURBS Book (Monographs in Visual Communication), second ed., *Springer-Verlag*, New York, 1997.

[35] G. Farin, Curves and Surfaces for CAGD, A Practical Guide, Fifth Edition. *Morgan Kaufmann Publishers* 1999.

[36] D.F. Rogers, An introduction to NURBS With Historical Perspective, *Academic Press*, 2001.

[37] J.A. Cottrell, T.J.R. Hughes, A. Reali, Studies of refinement and continuity in isogeometric structural analysis, *Computer Methods in Applied Mechanics and Engineering* 196 (2007) 4160-4183.

[38] C. Farhat, F.X. Roux, A method of finite element tearing and interconnecting and its parallel solution algorithm, *International Journal for Numerical Methods in Engineering* 32 (1991) 1205-1227.

[39] P. Gosselet, C. Rey, Non-overlapping domain decomposition methods in structural mechanics, *Archives of Computational Methods in Engineering* 13 (2006) 515-572.

[40] J.C. Passieux, P. Ladevèze, D. Néron, A scalable time-space multiscale domain decomposition method: adaptive time scale separation, *Computational Mechanics* 46 (2010) 621-633.

[41] Y. Bazilevs, M.C. Hsu, M.A. Scott, Isogeometric fluid-structure interaction analysis with emphasis on non-matching discretizations, and with application to wind turbines, *Computer Methods in Applied Mechanics and Engineering* 249-252 (2012) 28-41.

[42] A. Fritz, S. Hüeber, B. Wohlmuth, A comparison of mortar and Nitsche techniques for linear elasticity, *Calcolo* 41 (2004) 115-137.

[43] D. Schillinger, M. Ruess, The Finite Cell Method: A review in the context of higher-order structural analysis of CAD and image-based geometric models, *Archives of Computational Methods in Engineering* (2015) 1-65.

[44] A.P. Nagy, D. J. Benson, On the numerical integration of trimmed isogeometric elements, *Computer Methods in Applied Mechanics and Engineering* 284 (2015) 165-185.

[45] L. Kudela, N. Zander, T. Bog, S. Kollmannsberger, E. Rank, Efficient and accurate numerical quadrature for immersed boundary methods *Advanced Modeling and Simulation in Engineering Sciences* (2015) 2:10.

[46] O.C. Zienckewicz, R.L. Taylor, The Finite Element Method - The Basis, vol.1, *Butterworth-Heinemann*, 2005, sixth ed..

[47] J. Kiendl, Y. Bazilevs, M.C. Hsu, R. Wuüchner, K.U. Bletzinger, The bending strip method for isogeometric analysis of Kirchhoff-Love shell structures comprised of multiple patches, *Computer Methods in Applied Mechanics and Engineering* 199 (2010) 2403-2416.